Physics – Uspekhi **50** (3) 301 – 324 (2007)

CONFERENCES AND SYMPOSIA

PACS number: 01.10.Fv

Joint meeting of the Editorial Board of the Journal "Izvestiya Vuzov. Radiofizika" and the Scientific Council of the Institute of Applied Physics of the Russian Academy of Sciences dedicated to the ninetieth birthday of Vitalii Lazarevich Ginzburg (4 October 2006)

A joint meeting of the Editorial Board of the Journal "Izvestiya Vuzov. Radiofizika" and the Scientific Council of the Institute of Applied Physics of the Russian Academy of Sciences dedicated to the ninetieth birthday of Vitalii Lazarevich Ginzburg was held in the Conference Hall of the Institute of Applied Physics, Russian Academy of Sciences (Nizhnii Novgorod), on 4 October 2006. The following reports were presented at the session:

(1) **Zheleznyakov V V** (Institute of Applied Physics, Russian Academy of Sciences, Nizhnii Novgorod). "On the Nizhnii Novgorod school of Vitalii Lazarevich Ginzburg";

(2) **Andronov A A** (Institute of the Physics of Microstructures, Nizhnii Novgorod). "Chirality: optical rotation, the detailed balance principle, and life";

(3) **Bratman V L** (Institute of Applied Physics, Russian Academy of Sciences, Nizhnii Novgorod). "Fast moving radiators and their use in high-frequency electronics";

(4) **Derishev E V, Kocharovsky V V, Kocharovsky Vl V** (Institute of Applied Physics, Russian Academy of Sciences, Nizhnii Novgorod). "Cosmic accelerators for ultrahigh-energy particles";

(5) **Frolov V L, Bakhmet'eva N V, Belikovich V V, Komrakov G P** (Scientific-Research Radiophysical Institute (NIFRI) Federal State Scientific Organization, Nizhnii Novgorod), **Vertogradov G G, Vertogradov V G** (Rostov State University, Rostov-on-Don), **Kotik D S, Mityakov N A, Polyakov S V, Rapoport V O, Sergeev E N** (NIFRI, Nizhnii Novgorod), **Tereshchenko E D** (Polar Geophysical Institute of the Kola Science Center, Russian Academy of Sciences (PGI KSC RAS), Murmansk), **Tolmacheva A V, Uryadov V P** (NIFRI, Nizhnii Novgorod), **Khudukon B Z** (PGI KSC RAS, Murmansk). "Modification of the earth's ionosphere by high-power high-frequency radio waves."

A brief presentation of reports 2 – 5 is given below.

Uspekhi Fizicheskikh Nauk **177** (3) 315 – 340 (2007)
Translated by E N Ragozin; edited by A M Semikhatov

PACS numbers: 42.25.Ja, **87.10.+e**
DOI: 10.1070/PU2007v050n03ABEH006279

Chirality: optical rotation, the detailed balance principle, and life

A A Andronov

A chiral system is a system that has no mirror symmetry — a center or plane of inversion. The subject of the first part of my report — optical rotation — was not selected at random: the first scientific work by the author of this report (a 4 – 5th year student at that time) "On the natural rotation of the polarization plane of sound" [1], which was carried out at the suggestion of Vitalii Lazarevich, was concerned with the chirality problem.

Vitalii Lazarevich himself gave quite a bit of space to the natural rotation of the polarization plane in electrodynamics in his work dedicated to media with spatial dispersion [2]. In particular, in his report [3] he discussed the problem of boundary conditions in media with natural optical activity. This problem may also be formulated as follows: what takes place when a linearly polarized wave is (normally) incident on a naturally active medium? Two types of (phenomenological) boundary conditions were considered in Ref. [3]. With one type of boundary condition, the polarization becomes elliptic on reflection and with the other type it remains unchanged. What occurs 'in reality'? The situation is unclear.

As far as I know, there are only two papers in which an attempt was made to measure the rotation of a polarization plane at (normal) reflection from a naturally active medium [4, 5], the results being different. The effect is weak and, as noted in Ref. [3], any surface contamination (modification) can easily mask the result. And the phenomenology should not be in force. An example is found in the recent measurement of appreciably elliptic polarization in the reflection of linearly polarized light from a silicon surface that accommodated multiply (6×10^6 cm^{-2}) deposited chiral metallic microobjects [6]. In the absence of these objects, the effects of surface polarization variation are weak, and it is therefore expedient to study them using the methods of nonlinear optics.

The effects at a chiral boundary of semiconductors where quantum wells were grown were observed and investigated jointly by a group from the Ioffe Physicotechnical Institute

and Regensburg University (Germany). An investigation was made of the chiral rectification of terahertz radiation (i.e., the emergence of current along the semiconductor surface, whose direction depends on the sense of circular polarization): the circular photogalvanic and spin-galvanic effects [7, 8]. The authors termed them the 'bicycle' effects (Fig. 1): the circularly polarized photons impart angular momentum to spins (treadles), which produce, via the spin – orbit coupling, a current in the plane (bicycles ride), the current direction depending on the sense of circular polarization in this case. These investigations actually contain many interesting details showing how all this emerges: considered is the dependence on the crystal type, the type of quantum wells, the presence of a magnetic field, the angle of wave incidence, etc. These works are a continuation of research into the photogalvanic effect in chiral media (see Ref. [9]).

The second part of my report is some speculation on the following subject: why are biological macromolecules — proteins and DNA — uniformly chiral (equally left or right for all living beings). In his review of topical problems [10], Vitalii Lazarevich placed primary emphasis on the life sciences and considered them to be the currently principal ones: "On this planet, the last basic questions that remain unanswered are the following ones: how did life originate and how did thought originate?" In the paper mentioned above, he touched upon the question of 'reductionism' — "the feasibility of explaining the living on the basis of physics, the already known physics. This is the common problem of biologists and physicists." In what followed, Ginzburg noted that physicists would more and more engage in biology, that they should move into biology. This is a rather old motivation, of course. Outstanding physicists — M Delbrück, E Schrödinger, F Crick and others — had already gone in for biology with this motivation (see Ref. [11]). But now the question of such a propensity is even more acute.

We now turn to the principle of detailed balance. It has two aspects: (i) the equal number of transitions there and back in equilibrium and (ii) the symmetry of the probabilities for scattering there and back (which may be significant under nonequilibrium conditions) [12]. The former is always obeyed. Here, we are dealing with the latter aspect. At the time when Vitalii Lazarevich was Editor-in-Chief of the journal *Izv. Vyssh. Uchebn. Zaved., Radiofiz.*, published in Nizhnii Novgorod (then the city of Gorki), submitted to the journal was a manuscript (which was widely debated later)

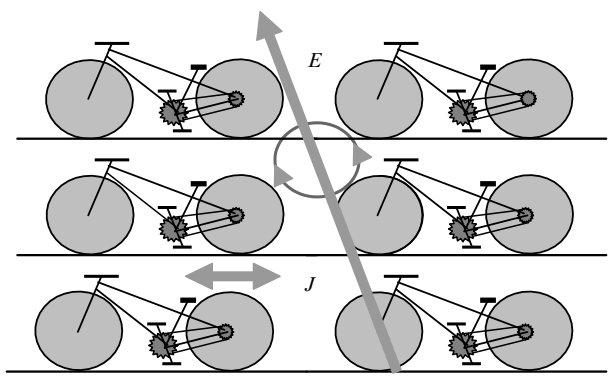

Figure 1. 'Bicycle' continuous current J under the action of circular polarization, which 'treadles': the circular photo- or spin-galvanic effects in chiral 2D structures near the semiconductor surface.

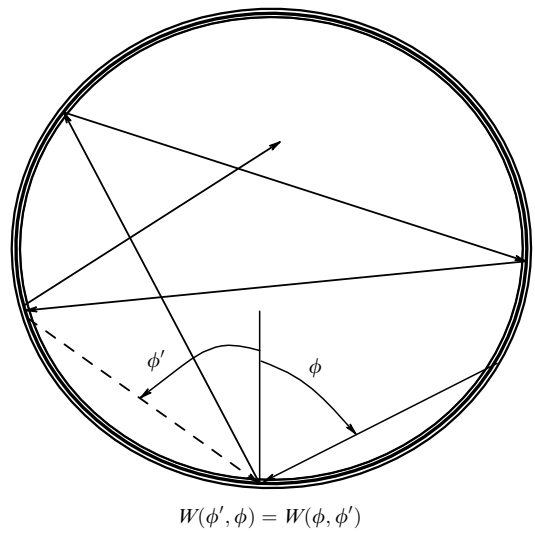

Figure 2. Knudsen gas in a rough cylinder subject to the condition of detailed balance at the surface in the case of equal probabilities W for the scattering forth and back.

concerned with the modeling of a Knudsen gas (the mean free path is much longer than the vessel dimensions, and molecules collide only with the rough walls in random elastic scattering) in a cylindrical tube (Fig. 2). The authors assumed a seemingly reasonable model whereby the fraction of specular reflection increased with the angle of incidence. And the gas began to rotate! The editors rejected the manuscript on the grounds that the scattering model assumed did not agree with the physical models that lead to the principle of detailed balance. Later there appeared a preprint from Dubna concerned with the modeling of ultracold neutron transfer in a cylindrical tube. Detailed balance in the scattering at the walls was taken into account and the neutrons did not rotate. And everybody calmed down.

But the principle of detailed balance is violated [9, 13 – 14]! However, this is not widely known (although this question is discussed in Ref. [12, Ch. 1, § 2], cf. also Ref. [13]): in the first Born approximation, the principle of detailed balance is always obeyed. Effects related to the violation of the detailed balance principle in scattering and those responsible for skew scattering are known in solid-state physics [14]. An example is provided by the anomalous Hall effect, which occurs due to the magnetization at which skew scattering occurs (and not due to the magnetic field).

What is to occur if we take a cylinder with a chiral roughness for the Knudsen gas (Fig. 3)? Will the gas rotate? This is unlikely. It is proven in Ref. [13] that in the chiral elastic scattering, too, the entropy increases and the gas supposedly must not rotate. It is likely that the relaxation to the mixed state is moderated. However, the author is unaware of works (examples) of this kind.

But if the transition to the mixed state is suppressed, this should (may) retard the transition to equilibrium of systems consisting of chiral elements. Is it not the reason for the chirality of living systems? Here, we do not discuss which spiral, left or right, occurs or what is the underlying: randomness (broken symmetry) or the action of an advantage factor (circularly polarized light, magnetic field, etc.) [15].

At the same time, Crick, who (jointly with D Watson) discovered the chiral DNA structure, never mentions (never

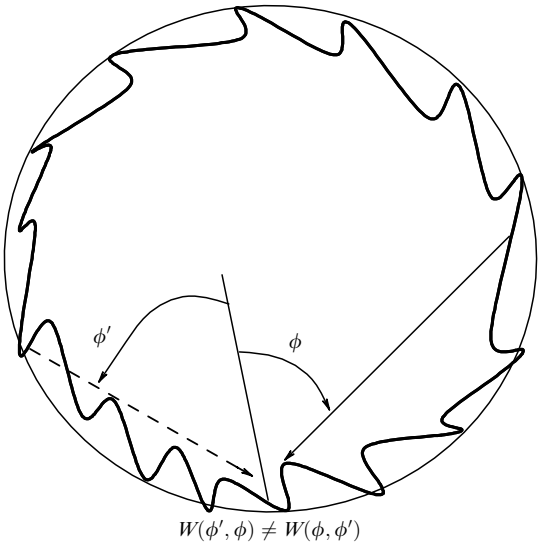

Figure 3. Detailed balance violation in the Knudsen gas in a chiral cylinder.

emphasizes) the chirality of biological molecules in his story of how he stayed interested in biology for 50 years [11]. Furthermore, he mocks at theoretical biologists who invoke a priori schemes and are preoccupied with them. He believes that evolution, or 'The Blind Watchmaker,' as referred to at the suggestion of the English pop biologist R Dawkins [16], is far from different schemes: an accident is more important. The blind watchmaker is seated in a chair in a field over which the wind is carrying parts of a watch. He is assembling a mechanism. He does not contemplate anything, he just fumbles about under the chair, finds something, inserts into the mechanism, and waits: will that do or not, will the Mechanism start going or not? Most likely, he chanced upon the left spiral and the mechanism started going, and all the remaining parts that fitted the mechanism also turned out to be left spirals. But the watchmaker could have chanced upon the right spiral or no spiral at all!

However, if spirals live longer, owing to the violation of the principle of detailed balance, they are to be in the 'initial broth,' from which the watchmaker picks up the components. Maybe therein lies, at least in part, the reason for the emergence of the chirality of biomolecules.

However, all this is speculation, of course.

The author expresses his gratitude to V V Ivanov, M A Novikov, and S V Sharov for helpful discussions.

References

1. Andronov A A *Izv. Vyssh. Uchebn. Zaved., Radiofiz.* **3** 645 (1960)
2. Agranovich V M, Ginzburg V L *Kristallooptika s Uchetom Prostranstvennoi Dispersii i Teoriya Eksitonov* (Crystal Optics with Spatial Dispersion, and Excitons) (Moscow: Nauka, 1965) [Translated into English (Berlin: Springer-Verlag, 1984)]
3. Ginzburg V L *Usp. Fiz. Nauk* **108** 749 (1972) [*Sov. Phys. Usp.* **15** 839 (1973)]
4. Luk'yanov A Yu, Novikov M A *Pis'ma Zh. Eksp. Teor. Fiz.* **51** 591 (1990) [*JETP Lett.* **51** 673 (1990)]
5. Bungay A R, Svirko Yu P, Zheludev N I *Phys. Rev. Lett.* **70** 3039 (1993)
6. Papakostas A et al. *Phys. Rev. Lett.* **90** 107404 (2003)
7. Ganichev S D et al. *Phys. Rev. Lett.* **86** 4358 (2001)
8. Ganichev S D et al. *Nature* **417** 153 (2002)
9. Belinicher V I, Struman B I *Usp. Fiz. Nauk* **130** 415 (1980) [*Sov. Phys. Usp.* **23** 199 (1980)]
10. Ginzburg V L *O Nauke, o Sebe i o Drugikh* (About Science, Myself, and Others) 3rd ed. (Moscow: Fizmatlit, 2003) [Translated into English (Bristol: IOP Publ., 2005)]
11. Crick F *What MAD Pursuit. A Personal View of Scientific Discovery* (New York: Basic Books, 1988) [Translated into Russian (Moscow – Izhevsk: IKI, 2004)]
12. Lifshitz E M, Pitaevskii L P *Fizicheskaya Kinetika* (Physical Kinetics) (Moscow: Nauka, 1979) [Translated into English (Oxford: Pergamon Press, 1981)]
13. Strurman B I *Usp. Fiz. Nauk* **144** 497 (1984) [*Sov. Phys. Usp.* **27** 881 (1984)]
14. Gantmakher V F, Levinson Y B *Carrier Scattering in Metals and Semiconductors* (Modern Problems in Condensed Matter Physics, Vol. 19, Eds V M Agranovich, A A Maradudin) (Amsterdam: North-Holland, 1987)
15. Gol'danskiĭ V I, Kuz'min V V *Usp. Fiz. Nauk* **157** 3 (1989) [*Sov. Phys. Usp.* **32** 1 (1989)]
16. Dawkins R *The Blind Watchmaker* (London: Penguin Books, 2006)

PACS numbers: 41.60.Cr, **52.59.–f**, 84.40.Ik

DOI: 10.1070/PU2007v050n03ABEH006280

Fast moving radiators and their use in high-frequency electronics

V L Bratman

In 1946, when discussing the possibilities for mastering the then hard-to-reach region of millimeter- and submillimeter waves, Ginzburg considered several generation techniques, which turned out to be highly efficient for a substantially broader spectrum of electromagnetic radiation. In Ref. [1], he proposed the use of Doppler frequency conversion of fast moving electron oscillators as "the most interesting and promising method."

Let an electron move with a translational velocity $\mathbf{v}_{||} = \boldsymbol{\beta}_{||} c$ and oscillate in the transverse direction with a frequency Ω in an electric field varying harmonically in time (Fig. 1). Then, at an angle θ to the direction of translational motion, the electron radiates at the frequency

$$\omega = \frac{\Omega}{1 - \beta_{||} \cos\theta} \,. \tag{1}$$

For an ultrarelativistic velocity $\beta_{||} \approx 1$, when the Lorentz factor γ of the electron is large, the Doppler frequency gain for the low-angle radiation is proportional to the squared particle energy, $\omega \sim \gamma^2 \Omega$, and may be quite high. For instance, for energies 5 MeV and 5 GeV, we obtain Doppler gains of the order of 10^2 and 10^8, respectively.

Ginzburg [1] also considered the possibilities that open up when the cyclotron and synchrotron radiation of an electron

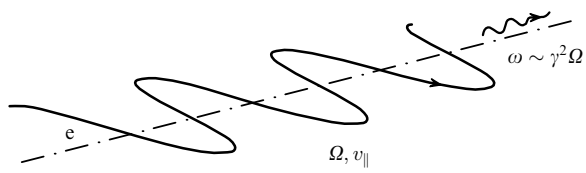

Figure 1. Idea of a 'dopplertron': an oscillating and rapidly moving charge radiates forward at frequencies that are many times higher than its oscillation frequency.

following a circular path in a uniform magnetic field is used. We note that in this case, too, the 'dopplertron' is easy to obtain by imparting to the electron a relativistic translational velocity along with the rotational one, such that the electron describes a helical trajectory (Fig. 2a). At the fundamental cyclotron resonance, its radiation frequency is given by formula (1), in which the oscillation frequency is equal to the relativistic electron cyclotron frequency $\Omega_B = \Omega'_B/\gamma$, where $\Omega'_B = eB/m$. In a strong magnetic field, it is easy to obtain a high Ω'_B frequency, but for large γ, because of a decrease in Ω_B, this method ranks in frequency below the dopplertron, for which the oscillation frequency is independent of the energy. At the same time, as emphasized in Ref. [1], the synchrotron radiation of a particle describing a circular path, which had just been discovered at that time, furnishes a peculiar example of a dopplertron with a very high frequency conversion ratio (Fig. 2b). As we now know, this dopplertron is highly important for different realms of physics and technology. In this case, the combined action of three effects — the relativistic angle transformation, which contracts the instantaneous radiation pattern to a narrow cone with the angle $\sim \gamma^{-1}$; the rotation of this pattern, which leads to a pulsed temporal structure of the radiation in a given direction; and the compression of a generated pulse by a factor of γ^2 due to the electron approaching the point of observation (the longitudinal Doppler effect) — has the consequence that the radiation peaks at a very high cyclotron harmonic with a frequency $\sim \gamma^3 \Omega_B$.

Along with the radiation of electrons rapidly moving in a vacuum, Ginzburg [1] also proposed the use of the radiation of electrons moving above a dielectric or in a dielectric channel (Cherenkov radiation and the Doppler effect in the presence of a decelerating medium). In these cases, obtaining short-wave radiation requires substantially lower particle energies.

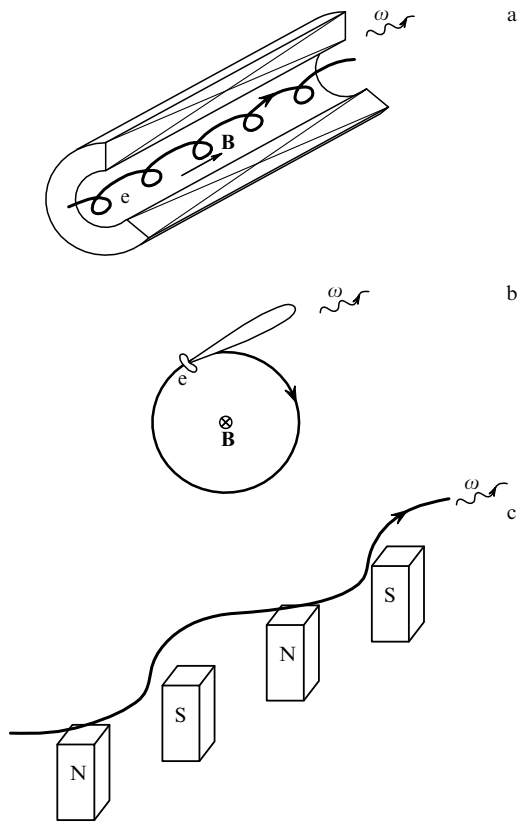

Figure 2. Examples of 'dopplertrons': cyclotron (a) and synchrotron (b) dopplertrons in a uniform magnetic field, an ondulator dopplertron in a spatially periodic magnetic field (c).

It is pertinent to note that several years later, the British physicist Motz [2] also proposed, independently of Ref. [1], the use of the Doppler effect for the emission of short-wave radiation. Furthermore, Motz proposed a highly efficient technique of particle oscillation buildup in a spatially periodic magnetic system producing a field transverse to the direction of particle motion — a static magnetic wave (Fig. 2c). These devices, which impart a periodic shape to a thin electron beam, have come to be known as ondulators (from the French onde — wave). It was not long before the Doppler-converted emission of isolated particles was discovered in diverse situations and different frequency regions. For instance, coherent Bremsstrahlung radiation was discovered in crystals, which emerges in the particle motion at a specific angle in an electrostatic ondulator produced by the fields of periodically located atoms. More recently, a discovery was made of a highly directional X-ray and gamma radiation of ultrarelativistic positrons and electrons related to another type of motion in crystals, channeling, which is accompanied by relatively low frequency transverse oscillations in the averaged atomic field.

Devices relying on frequency conversion in the photon backscattering by electrons (the inverse Compton effect), in which the pump wave field is used as the ondulator, may also be classed with dopplertrons. Another important example is provided by the Smith – Purcell radiation of particles moving rectilinearly above a periodic structure. The simplest interpretation of this effect is commonly given also in the spirit of a dopplertron and consists in considering an oscillating and rapidly moving dipole made up of the charge and its (quasistatic) image in the structure. The radiation of a charge penetrating through a periodic plate stack allows a similar explanation.

All the methods considered above involve individual (spontaneous) emission by particles or prepared compact bunches with dimensions smaller than the radiation wavelength. Preparing these bunches was a highly intricate problem, and much effort was mounted to do it in the 1950s. At the same time, these years saw the rapid development of electric vacuum microwave devices such as klystrons, magnetrons, traveling-wave tubes (TWTs), and backward-wave oscillators (BWOs), in which electrons are automatically[1] grouped in compact bunches, resulting in their collective (stimulated) emission. All these devices enabled generating radiation in the millimeter range for relatively low voltages, and it has even been possible to attain a wavelength of 0.2 mm with the help of a BWO. It is significant that the synchronous interaction (the Cherenkov or the transition interaction, which reduces to it) of particles with slow waves, which for low voltages requires electrodynamic systems with small-scale elements, is realized in these devices. The electrons must then travel at a very small distance from the decelerating systems (instead of the dielectrics proposed in Ref. [1], periodic metal structures are typically used) or through narrow gaps. Owing to wall overheating or the risk of a microwave breakdown, this leads to a rapid lowering of the output power P of the

[1] The operation of high-frequency charged-particle accelerators is also based on particle self-bunching.

above devices with decreasing the radiation wavelength λ: $P \propto \lambda^2$ at best.

Entirely new opportunities opened up when ensembles of electron oscillators were used as the active medium in short-wave vacuum devices [3]. To realize the stimulated (Bremsstrahlung) particle radiation in these electron lasers and masers, the fast eigenmodes of resonators and waveguides with smooth walls can be efficiently used. This is possible, in particular, in highly selective open large-volume electrodynamic systems where electrons can move away from the walls (and even in open space). Following a prehistory[2] rich in ideas and inventions (see Ref. [3]), the 1950s saw the introduction of two versions of electron masers, which are under active development at the present time: ubitrons [4] and cyclotron-resonance masers (CRMs, see, Ref. [3]).

Ubitrons (derived from 'undulated beam interaction') are a direct result of the elaboration of Ginzburg's and Motz's ideas towards obtaining stimulated emission from an electron beam propagating through a magnetostatic ondulator and interacting with the field of a waveguide or a resonator. In the 1970s, ubitrons took a leap into the 3 – 10 μm wavelength range [5, 6] to obtain a more spectacular name — free-electron lasers and masers (FELs and FEMs). This was the first and so far the only classical generator of coherent electromagnetic radiation that encroached so deep into the realm of quantum devices and was capable of competing with them in many cases (in what follows, we use the terms FEL and FEM in reference to all devices based on the Doppler-converted stimulated emission of rapidly moving electron oscillators).

We consider the principle of operation of an FEL ubitron (Fig. 3) in greater detail. In this device, an electron moves with a translational velocity $v_{\|}$ lower than the phase wave velocity, but its transverse oscillations under the action of the ondulator field occur in phase (at resonance) with the wave. This signifies the proximity of the phase $\omega t - k_{\|} z(t)$ of particle oscillations in the wave to the phase $\Omega_{\mathrm{u}} t$ of oscillations in the ondulator field, which gives resonance condition (1). Here, $\Omega_{\mathrm{u}} = 2\pi v_{\|}/d$ is the frequency of electron 'collisions' with field periods. The electric field of the wave works on the oscillating electron, while the magnetic wave field acts on its transverse motion and produces a resonance longitudinal force, which groups the particles as this occurs under the action of a longitudinal electric field of the slow wave in a TWT. This analogy becomes even more transparent when relation (1) is represented in the equivalent form of the synchronism condition for the electron and the field of a slow combination wave produced by the high-frequency wave and the ondulator field (magnetostatic wave with a wavenumber $k_{\mathrm{u}} = 2\pi/d$ and a zero frequency):

$$\omega = (k_{\|} + k_{\mathrm{u}})\, v_{\|} \,. \tag{2}$$

In this case, the frequency, the wavenumber, and the phase velocity of the combination wave are respectively equal to the high-frequency wave frequency ω, $k_{\|} + k_{\mathrm{u}}$, and $\omega/(k_{\|} + k_{\mathrm{u}})$, while the amplitude is proportional to the product of the amplitudes of the high-frequency and magnetostatic waves. According to relation (2), the phase velocity of the combination wave in the ubitron is therefore equal to the translational particle velocity (more precisely, should be close to it). Under the action of the wave, a part of the electrons is decelerated and a part of them is accelerated in the longitudinal direction. This process, which is responsible for particle grouping in compact bunches like ordinary TWTs and klystrons, is inertial in character and may continue even in regions where the high-frequency field is absent. This approach and the analogy with a TWT are also easily extended to the motion and stimulated emission of electrons in the field of a pump wave with a frequency ω_{i} and the longitudinal wavenumber k_{i}, i.e., to the scattering of a wave (photons) by electrons:

$$\omega - \omega_{\mathrm{i}} = (k_{\|} + k_{\mathrm{u}})\, v_{\|} \,. \tag{3}$$

The backscattering from an ultrarelativistic charge exemplifies the reflection of a wave by a mirror moving fast towards it, which was considered by Einstein.

For a relatively small variation in the energies of particles, their grouping under the action of the wave and the energy exchange with it in an FEL are described by precisely the same equations as in a TWT. In particular, for the stationary regime of an FEL oscillator with a high-Q resonator, in which the wave amplitude may be considered constant, the equations of motion of the beam electrons are brought to the form [7]

$$\frac{\mathrm{d}w}{\mathrm{d}\zeta} = \varkappa\, \mathrm{Re}\, a \exp(\mathrm{i}\vartheta) \,, \quad \frac{\mathrm{d}\vartheta}{\mathrm{d}\zeta} = \mu w + \delta \,, \tag{4}$$

which coincides with the equations for the oscillator version of a TWT. Here, w and ϑ are the relative energy variation of a particle and its phase relative to the combination wave, ζ is the dimensionless coordinate, $\varkappa$ is the electron – wave coupling coefficient proportional to the transverse particle velocity, a is the dimensionless amplitude of the combination wave, $\mu \approx \gamma_0^{-2}$ is the nonisochronity parameter of particle oscillations in the wave, and δ is the dimensionless detuning from the exact synchronism described by relations of type (1) – (3). By differentiating the equation for the electron phase ϑ with respect to ζ and using the equation for the energy w, it is easy to verify that the nonlinear system of equations (4) is equivalent to the equation of a mathematical pendulum.

A stationary electron beam in which particles are uniformly distributed in the initial phase ϑ_0 from 0 to 2π is normally fed to the oscillator input. For a negligibly small particle energy spread, this corresponds to the initial condition

$$w(0) = 0 \,, \quad \vartheta(0) = \vartheta_0 \,. \tag{5}$$

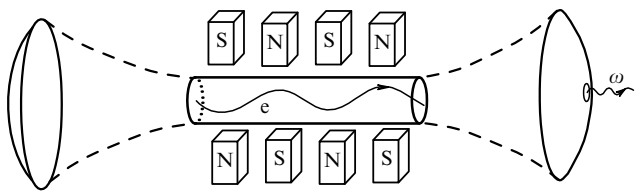

Figure 3. Scheme of a free-electron laser with an ondulator and an open resonator. Electrons are grouped in the longitudinal direction (as in a traveling-wave tube) under the action of the combination wave produced by the radiated wave and the spatially periodic ondulator field (magnetostatic wave).

[2] Interestingly, the first electron maser (a triode with a positive grid — a Barkhausen – Kurtz oscillator) was realized shortly after Einstein introduced the notion of spontaneous and stimulated emission of quantum systems, i.e., long before the advent of the 'laser era.'

Integrating system of equations (4) with boundary conditions (5) for a small amplitude a up to second-order terms and averaging the result over the initial particle phase, we obtain the efficiency of energy exchange between the electron oscillators and the wave in the small-signal approximation as

$$\eta_{\text{s.s.}} = (\varkappa a)^2 \mu \xi^3 \varphi'(\psi)\,, \tag{6}$$

where $\varphi(\psi) = (1 - \cos\psi)/2\psi^2$ is the function proportional to the intensity of the spectrum of the high-frequency force (in this case, 'a stopped sinusoid') acting on an electron in its transit through the resonator, $\psi = \delta\xi$ is the particle transit angle relative to the wave, and ξ is the dimensionless length of the interaction space. According to expression (6), the electrons transfer their energy to the wave in the main zone of transit angles $-2\pi < \psi < 0$, where the particle velocities exceed the phase velocity of the combination wave and $\varphi'(\psi)$ is positive.

Asymptotic nonlinear equations (4), as well as their generalization to the case of a variable-amplitude high-frequency wave, apply to all kinds of FELs and other devices based on various mechanisms of inertial particle grouping (see Ref. [8]). The possibility of a common approach on the basis of universal equations significantly simplifies comparison of different devices with each other.

The question of the efficiency attainable in an FEL is significant for applications. In the approximation of a low particle energy variation, the efficiency is found by integration of Eqns (5) in the regime of a relatively large signal. Here, we restrict ourselves to simple estimates that can be derived from the equations themselves or from their corresponding phase plane (Fig. 4), or directly from the conditions that particles come out of resonance (1) with the wave. All these methods give the following estimates for the energy exchange between electrons and a fixed wave, as well as for the admissible particle energy spread:

$$\eta \sim \frac{\Delta\gamma}{\gamma} \sim \frac{1}{2N}\,, \tag{7}$$

where N is the number of particle oscillations in the ondulator. Similar estimates are obtained for the frequency band generated in the FEL and the optimal detuning from resonance:

$$\frac{\Delta\omega}{\omega} \sim \delta \sim \frac{1}{2N}\,. \tag{8}$$

For very high N, the requirements on the spread become quite stringent, while exciting the resonator for small N requires very high currents. In all FELs, the interaction length and the number of particle oscillations are therefore rather high and the efficiency in the simplest scheme is rather low.

However, there are several ways to radically increase the efficiency up to quite high values of several dozen percent, which was achieved in experiment. The basic idea of this improvement [9] was obtained by inverting the principle of operation of high-frequency accelerators; it was also proposed in papers on TWTs [10]. Unlike in the above method involving the 'conventional' regime of inertial particle grouping, whereby saturation occurs at the exit of the electron bunches from synchronism with the wave (Fig. 4a), in this method a substantial fraction of electrons is captured into the potential well formed by the wave (a 'bucket' formed by separatrices, Fig. 4b), and then the particles remain in synchronism with the wave due to the FEL parameter

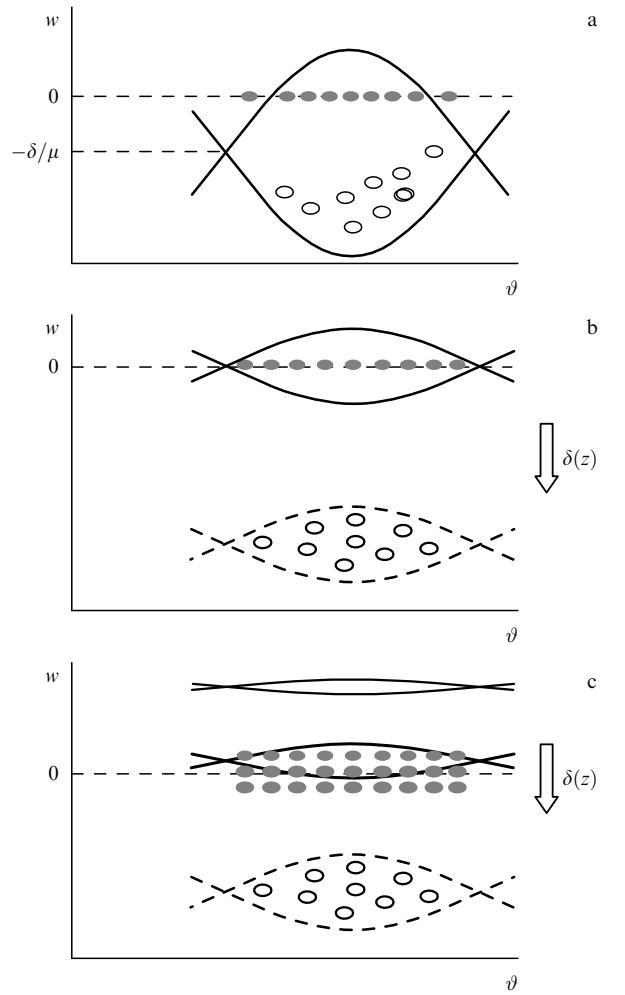

Figure 4. Comparison of free-electron lasers with constant or lengthwise-varied ondulator parameters in the phase plane 'relative energy variation — electron phase'. For constant parameters (a), particles assemble in a bunch, which sinks to the bottom of the 'bucket' formed by the wave with a relatively low amplitude and imparts a small energy fraction to it (the conventional low-efficiency regime of inertial particle grouping). For slowly varying parameters (b, c), the particles are captured into the bucket and adiabatically decelerated with it to donate a substantial energy fraction to the wave (the capture regime with a high efficiency). For a high-current electron beam and a rapid wave amplification on reaching particle – wave resonance (c), the blowing-up bucket is able to capture different beam fractions with a wide velocity spread.

profiling lengthwise to the system and are smoothly decelerated together with the bucket. Also proposed, as a development of this trick, was the 'blowing-up bucket' technique [11] (Fig. 4c), which permits, according to calculations, using a beam with a wide parameter spread and obtaining wide amplification bands.

Quite interesting regimes were realized in FELs, which were previously unknown in vacuum electronics. In particular, the first infrared generator [5] already involved longitudinal resonator mode locking via periodic injection of virgin electron bunches in time with the circulation of a short electromagnetic pulse (the 'slice' of the electromagnetic field formed by a large number of modes) in the resonator. Vinokurov and Skrinskii [12] proposed and later realized a version of an FEL in the form of a so-called optical klystron, in which particle energy modulation and the energy extraction from the bunches occur in short ondulator sections and

the transverse magnetic field in a gap between these sections is used to speed up the electron bunching. Several FELs use highly selective large-volume electrodynamic systems, which enable exciting a single mode at a high power level and at the same time using one of the main FEL virtues, the capability of radiation frequency tuning over an extremely wide range.

To date, a large number of FELs of different types have been realized, from the millimeter range to the vacuum ultraviolet range (see Ref. [13]); several of them have been in successful operation for many years, enabling the pursuit of diversified research. A high-power terahertz FEL was recently developed in Russia [14]. In the 1980s, FELs were considered essential elements of the so-called Strategic Defense Initiative. Today, the most ambitious projects are aimed at producing coherent X-ray radiation (see, e.g., Ref. [15]). Among its stated fantastic potentialities are, in particular, shooting chemical reactions and the response of materials and biomolecules with atomic resolution. Owing to the absence of sufficiently strong input signal sources, the planned X-ray FELs are to use the intrinsic e-beam noise amplification self-narrowing in frequency — the mode of self-amplified spontaneous emission (SASE) demonstrated in the long-wavelength ranges. Producing radiation in the X-ray range requires electron energies of several gigaelectronvolts. Such beams with pulsed kiloampere currents are produced in linear accelerators several kilometers long, and the particle oscillation is effected in ondulators several hundred meters long.

It should be remembered that the field in the simplest ondulator (Fig. 2c) decreases exponentially with the distance from the magnets. To weaken this effect, two slightly spaced parallel magnet systems (Fig. 3) or helical current ondulators with a double winding or more complex systems are used. It has been possible to make ondulators with periods down to several millimeters or even shorter; in practice, however, ondulators with periods less than several centimeters are infrequently employed. Accordingly, beams with particle energies above 1 MeV are used to obtain lasing in the short-wavelength part of the millimeter range. Ondulators in the form of a pump wave permit forming transversely uniform fields with a short period; however, obtaining particle oscillations with a sufficiently high amplitude requires very high pump powers. It is much simpler to obtain short periods of curvilinear particle motion for producing lasing in the millimeter and submillimeter ranges by using a uniform magnetic field for pumping and the stimulated cyclotron radiation of electron beams for the radiation mechanism. This Doppler version of a CRM is called a cyclotron autoresonance maser (CARM) [8, 16].

The cyclotron autoresonance effect [17, 18] consists in the exact resonance condition (1), if initially satisfied, being automatically maintained for an electron that travels in a uniform magnetic field and the field of a wave propagating along the magnetic field in a vacuum. Indeed, in each event of elementary interaction with the wave, the energy and translational momentum of the electron change by fixed values $\hbar\omega$ and $\hbar\omega/c$. For finite variations in the quantities, we therefore obtain $\Delta E/\Delta p_{||} = c$. This implies the conservation of the left-hand side of the relation

$$\gamma\,(1-\beta_{||})\,\omega = \Omega'_B\,, \tag{9}$$

which is equivalent to condition (1), and the possibility for unlimited (for a constant wave amplitude) electron acceleration. Under these conditions, however, the nonisochronity due to the relativistic dependence of the cyclotron frequency on the particle energy (the nonequidistance of Landau energy levels in the quantum interpretation), which is responsible for the azimuthal particle displacement in the Larmor circle, is exactly compensated by the nonisochronity of longitudinal particle oscillations under the action of the magnetic field of the wave (recoil in the emission of a photon) [19]. An electron ensemble therefore behaves as an ensemble of linear oscillators. Accordingly, the stimulated absorption in it prevails over emission.

For the emission to prevail, the above cancellation should be slightly disturbed [16] by using a fast wave in whose field the particle oscillation nonisochronity parameter $\mu = (c^2k_{||}^2/\omega^2) - 1$, which includes both mechanisms, is nonzero. In this case, the deviation from resonance may be small even for appreciable variations in the cyclotron frequency and translational particle velocity, which allows obtaining a high efficiency even for a large length without profiling the parameters of the system [20]. However, this is possible only for a very narrow particle velocity spread and a high selectivity of the electrodynamic system. Each of these goals is rather hard to achieve considering that the nonisochronity parameter in a CRM strongly depends on the phase velocity of the eigenwave of the electrodynamic system. Among these waves, the occurrence of 'parasitic' waves, which propagate almost transversely to the magnetic field and accordingly have high phase velocities in the direction of particle motion, is practically inevitable. However, the operation by precisely these waves is extremely attractive and they are very efficiently employed in another, much more widely used and highly efficient CRM version, the gyrotron [3, 21].

The longitudinal Doppler effect is practically absent in the gyrotron (Fig. 5), which deprives this device of oscillation frequency conversion but in return affords it its main virtue — the high nonsensitivity to particle velocity spread, which in most cases outweighs the above drawback. Even for a low particle energy, gyrotron operation is entirely based on the relativistic effect discussed in the foregoing, the nonisochronity of electron cyclotron rotation. Owing to the nonisochronity, the particles group in compact bunches in

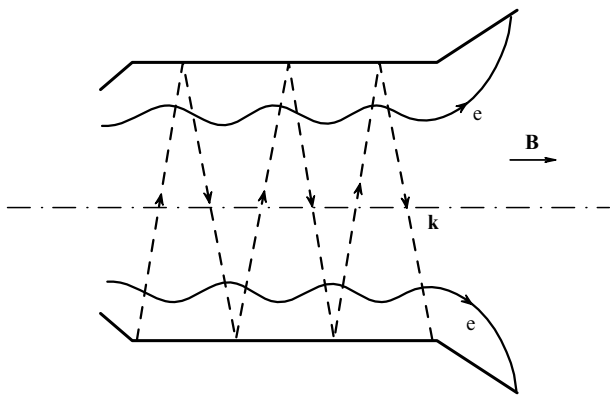

Figure 5. Schematic of a gyrotron with an open resonator in the form of a leg of a weakly irregular cylindrical waveguide with a tubular electron beam. The partial waves that make up the field of the working mode propagate almost transversely to the magnetic field, which leads to a small Doppler correction and a high nonsensitivity to the particle energy spread. Under the action of the wave, electrons group in azimuthal bunches owing to the relativistic nonisochronity of cyclotron rotation.

the Larmor circles under the action of a 'seed' signal, and then the bunches impart their rotational energy to the wave. The effectiveness of these processes may be so high that modern gyrotrons range up to 50% in efficiency.

For the electrodynamic systems in gyrotrons, selective resonators in the form of sections of weakly irregular cylindrical waveguides are typically used (see Fig. 5), with the highest-Q oscillations being those with one longitudinal variation and with the frequencies closest to the cut-off waveguide frequencies. These modes correspond to the least values of the longitudinal wavenumber and the Doppler correction to the frequency, and are therefore least sensitive to electron velocity spread. To provide the optimal value of the force acting on the particles, as well as to reduce the risk of a high-frequency breakdown at the walls and decrease their heating, high-power gyrotrons involve resonators that are many times greater in diameter than the working wavelength and working modes with a complex transverse structure. It is remarkable that using the resonance in a magnetic field with a high degree of uniformity and injecting the electron beam into the domain with a high effective mode field, it has been possible to excite these modes with only a small admixture of undesirable waves.

Gyrotrons intended for plasma heating are broadly used in controlled thermonuclear fusion facilities to provide enormous power, of the order of 1 MW, in a cw oscillation mode at frequencies 30 – 170 GHz. Furthermore, lower-power 5 – 300 GHz gyrotron oscillators and amplifiers find technological applications, as well as applications in radars, spectroscopy, and diagnostics of various media. Recently, in the prototypes of pulsed gyrotrons, it has been possible to obtain oscillation at the frequency 1 THz. Obtaining this frequency requires a hard-to-attain magnetic field, 36 T when operating at the fundamental cyclotron resonance. In recent years, efforts have been intensified to obtain generation at higher harmonics, which requires lower magnetic fields.

Reverting to the beginning, we note that the millimeter wavelength range and, to a large extent, the submillimeter range are presently mastered by electronic devices based on various principles. In accordance with Ginzburg's predictions [1], the role of devices that rely on the emission of electron oscillators is great in these ranges. True, the stimulated radiation of previously unphased particles resulting from their self-bunching but not the radiation of preformed electron bunches immediately considered in Ref. [1] has turned out to be most efficient. The devices based on the stimulated radiation of electron oscillators already provide coherent high-power radiation not only in the above ranges but also up to the vacuum ultraviolet range, and may allow obtaining coherent X-ray radiation in the near future. The analysis of elementary mechanisms of emission by 'free' electrons and the new ideas advanced in Ref. [1] have had an impact on the development of all high-frequency electronics.

References

1. Ginzburg V L *Izv. Akad. Nauk SSSR, Ser. Fiz.* **11** 165 (1947)
2. Motz H *J. Appl. Phys.* **22** 527 (1951)
3. Gaponov A V, Petelin M I, Yulpatov V K *Izv. Vyssh. Uchebn. Zaved., Radiofiz.* **10** 1414 (1967) [*Radiophys. Quantum Electron.* **10** 794 (1967)]
4. Phillips R M *IRE Trans. Electron Devices* **ED-7** 231 (1960)
5. Elias L R et al. *Phys. Rev. Lett.* **36** 717 (1976)
6. Deacon D A G et al. *Phys. Rev. Lett.* **38** 892 (1977)
7. Colson W B *Phys. Lett. A* **59** 187 (1976)
8. Bratman V L, Ginzburg N S, Petelin M I *Opt. Commun.* **30** 409 (1979)
9. Kroll N, Morton P, Rosenbluth M, in *Free-electron Generators of Coherent Radiation* (Physics of Quantum Electronics, Vol. 7, Eds S F Jacobs et al.) (Reading, Mass.: Addison-Wesley Publ. Co., 1980) p. 89
10. Belyavskii E D *Radiotekh. Elektron.* **16** 208 (1971)
11. Savilov A V *Phys. Rev. E* **64** 066501 (2001)
12. Vinokurov N A, Skrinskii A N, Preprint No. 77-59 (Novosibirsk: Institute of Nuclear Physics of the Siberian Branch of the Academy of Sciences of USSR, 1977)
13. Colson W B, Williams B W, in *FEL 2004: Proc. of the 26th Intern. Free Electron Laser Conf. and 11th FEL User Workshop, Aug. 29 – Sept. 3, 2004, Trieste, Italy* (Eds R Bakker et al.) (Trieste: Comitato Conf. Elettra, 2005) p. 706
14. Bolotin V P et al., in *FEL 2004: Proc. of the 26th Intern. Free Electron Laser Conf. and 11th FEL User Workshop, Aug. 29 – Sept. 3, 2004, Trieste, Italy* (Eds R Bakker et al.) (Trieste: Comitato Conf. Elettra, 2005) p. 226
15. Schwarz D S, in *FEL 2004: Proc. of the 26th Intern. Free Electron Laser Conf. and 11th FEL User Workshop, Aug. 29 – Sept. 3, 2004, Trieste, Italy* (Eds R Bakker et al.) (Trieste: Comitato Conf. Elettra, 2005) p. 85
16. Petelin M I *Izv. Vyssh. Uchebn. Zaved., Radiofiz.* **17** 902 (1974) [*Radiophys. Quantum Electron* **17** 686 (1974)]
17. Kolomenskii A A, Lebedev A N *Dokl. Akad. Nauk SSSR* **145** 1259 (1962) [*Sov. Phys. Dokl.* **7** 745 (1963)]
18. Davydovskii V Ya *Zh. Eksp. Teor. Fiz.* **43** 886 (1962) [*Sov. Phys. JETP* **16** 629 (1963)]
19. Gaponov A V *Zh. Eksp. Teor. Fiz.* **39** 326 (1960) [*Sov. Phys. JETP* **12** 232 (1961)]
20. Bratman V L et al. *Phys. Rev. Lett.* **75** 3102 (1995)
21. A V Gaponov-Grekhov (Ed.) *Girotron* (Gyrotron) Collection papers (Gorky: IPF AN SSSR, 1981)

PACS numbers: **96.50.S** –, 98.70.Sa

DOI: 10.1070/PU2007v050n03ABEH006281

Cosmic accelerators for ultrahigh-energy particles

E V Derishev, V V Kocharovsky, Vl V Kocharovsky

1. Introduction

Ginzburg made a significant contribution to solving the problem of the origin of cosmic rays, in particular, by analyzing the synchrotron radiation of their constituent high-energy electrons, developing the concept of the galactic cosmic ray halo, and investigating several other problems (see his review Ref. [1] and the works of his school, e.g., Refs [2, 3]). Many questions still remain open in this area; however, as before, according to Ref. [1], "the most important problem yet to be solved in cosmic ray astrophysics is the origin of cosmic rays of ultrahigh energy." This problem is discussed in our report, which is based on previously published works [4 – 6].

The cosmic ray composition is dominated by positive-charged ions, primarily protons, while the particle distribution function over energies, $\mathrm{d}N/\mathrm{d}E$, is described with a high degree of accuracy by a power-law dependence with a break (a knee): $\mathrm{d}N/\mathrm{d}E \propto E^{-2.7}$ for energies below $\approx 3 \times 10^{15}$ eV and $\mathrm{d}N/\mathrm{d}E \propto E^{-3}$ for higher energies (see, e.g., review Ref. [7]). The properties of cosmic rays with energies up to 10^{17} eV, which have galactic origin and are produced primarily in

supernova explosions, were considered, e.g., in Ref. [3] and are not discussed below.

The question of the highest energy of cosmic rays is still unanswered. To date, particles with energies up to 10^{20} eV have been detected. Observations at higher energies encounter serious difficulties, because the expected flux is less than one particle per square kilometer per century. The sources of these particles are not known, either; however, the extragalactic origin of ultrahigh-energy cosmic rays ($\gtrsim 10^{18}$ eV) may be considered established. Two circumstances argue in favor of this conclusion. First, protons with energies above 10^{18} eV and heavy ions with energies $\gtrsim 2 \times 10^{19}$ eV are weakly deflected by the magnetic field of our galaxy, and therefore their production in galactic sources would lead to an increase in the flux in the direction towards the galactic nucleus and/or in the galactic disk plane, whereas the observed cosmic ray flux is virtually isotropic. Second, recently obtained evidence indicates that the cosmic ray spectrum steeply drops for energies higher than 5×10^{19} eV [8], which is consistent with predictions made by Kuz'min and Zatsepin [9] and Greisen [10]. The effect they point out is that protons with energies above $\gtrsim 5 \times 10^{19}$ eV rapidly (on the cosmological time scale) lose energy due to the interaction with the microwave background radiation and reach us only from distances $\lesssim 50$ Mpc. This leads to a strong decrease in the observed flux of particles with energies of the order of 10^{20} eV if they are produced primarily by distant sources.

We start from the natural hypothesis that the ultrahigh-energy cosmic rays originate in the acceleration of ions in the electromagnetic fields of astrophysical objects. An alternative hypothesis (termed 'top-down') requires invoking presently unknown physical phenomena and states that the source of cosmic rays is the decay of superheavy particles of dark matter [11]; produced in this case are the highest-energy cosmic rays, which subsequently lose their energy to form the observed distribution.

The fact that particles with energies of the order of 10^{20} eV exist in space should not come as a surprise. The cosmic plasma is far from thermodynamic equilibrium, and the effective temperature corresponding to its large-scale motions exceeds the energy of cosmic ray particles by several dozen orders of magnitude. A fraction of the ions would be expected to accelerate to very high energies due to multiple collisions with moving cosmic plasma clouds. This mechanism was advanced by Fermi [12]. With the knowledge of the lifetime of the cosmic rays in our galaxy, it is possible to calculate the required source power. It turns out to be of the same order of magnitude as the time-averaged power of supernova explosions, which are the main driving force of turbulence in the interstellar medium. This circumstance led to the hypothesis that supernova explosions are the main source of cosmic rays [13]. After the discovery of the diffusive particle acceleration at a shock front [14, 15] and the emergence of numerous detailed calculations (see, e.g., Ref. [16]), it became clear that cosmic rays emerge early in the existence of a supernova remnant, while the shock generated in its explosion remains strong. This picture was borne out experimentally (see, e.g., Ref. [17]): hard gamma-ray radiation caused by the inelastic collisions of accelerated cosmic rays with interstellar medium particles was detected from supernova remnants.

Shock waves in supernova remnants are capable of accelerating protons to an energy approximately corresponding to the knee in the cosmic ray spectrum and the nuclei of heavy elements with the charge $q = Ze$ can be accelerated to a Z-times higher energy, which ranges up to $\sim 10^{17}$ eV for iron. The further acceleration is impeded by the limited size of the remnant and the magnitude of the magnetic field in it: the high-energy ions are not confined by the magnetic field and escape from the shock. Explaining the origin of ultrahigh-energy cosmic rays requires objects of greater size or with stronger electromagnetic fields. But introducing such objects leads to problems, which may be divided into two groups.

First, these are mutually antithetic requirements on the electromagnetic fields in the objects of interest. On the one hand, they should be strong enough to allow acceleration to the required energy in a time during which the particles are confined in the accelerator. On the other hand, they should be sufficiently weak so as not to lead to excessive radiative losses. As shown in Section 2, the simultaneous fulfillment of the above requirements significantly limits the minimal size of the accelerator and dictates the minimal energy stored in its field. Second, the acceleration mechanism should be efficient enough: owing to the limited power of appropriate astrophysical objects, they should transfer a significant fraction of their power to ultrahigh-energy cosmic rays. The converter acceleration mechanism considered in Section 3, which is a Fermi-type mechanism, meets this requirement. In Section 4, we discuss several peculiarities of the energy gain and radiation for particles accelerated by this mechanism in relativistic plasma flows.

2. Minimal requirements on cosmic accelerators

The mere existence of the ion acceleration mechanism and the fulfillment of its realization conditions are not sufficient for an astrophysical object to become a source of ultrahigh-energy cosmic rays. It is also required that the acceleration power exceed the total particle energy loss rate. A large number of processes responsible for energy losses by high-energy ions may be eliminated or brought to an admissible low level by appropriate selection of the astrophysical object — the source of cosmic rays. Only the losses related to the accelerating electromagnetic field itself are fundamentally unavoidable. It is these losses that impose fundamental limitations on the parameters of cosmic accelerators.

We consider a particle acceleration region of size R. It can be naturally assumed that nothing like linear accelerators exists in space, and hence the curvature radius of magnetic and electric field lines is smaller than or of the order of R.

The accelerated particle trajectory depends on the energy loss rate. A high radiative loss rate leads to a rapid decrease in the particle momentum component transverse to the field direction and compels the particle to move along the field line. In the case of slow losses, the field geometry has only a weak effect on the particle trajectory at the angle $\sim 45°$ with the field lines.

A particle accelerates to the limiting energy defined by the smallest of two values: either the work of the accelerating force in a time during which the particle is confined in the accelerator or the energy value at which the energy loss rate $\dot{\varepsilon}_{\rm rad}$ becomes comparable with the acceleration rate. The balance of acceleration and losses is reached for

$$\dot{\varepsilon}_{\rm rad} = \frac{2}{3}\,\gamma^4\,\frac{q^2}{R^2}\,c = \eta q B c \qquad (1)$$

in the case where curvature radiation [2] prevails (assuming that the particle moves along an arc of radius R) or for

$$\dot{\varepsilon}_{\rm rad} = \frac{2}{3}\,\gamma^2 \left(\frac{q^2}{mc^2}\right)^2 c\left(B_\perp^2 + E_\perp^2\right) = \eta q B c \tag{2}$$

in the case where synchrotron or Bremsstrahlung radiation prevails. Here, γ is the Lorentz factor of the particle, m is its mass, $B_\perp$ and $E_\perp$ are the rms magnitudes of the field components perpendicular to the particle momentum, and η is the dimensionless acceleration rate, i.e., the ratio of the mean accelerating electric field $E_{\rm eff}$ to the magnetic one.

Comparing Eqns (1) and (2) shows that the curvature radiation leads to lower (and hence more favorable to acceleration) radiative losses when the particle energy $\varepsilon = \gamma mc^2$ satisfies the condition

$$\varepsilon < qR\sqrt{B_\perp^2 + E_\perp^2}\,. \tag{3}$$

There is no way of violating condition (3), because this would lead, somehow or other, to a contradiction: either the particle gyroradius $r_{\rm H} = \varepsilon/(qB_\perp)$ turns out to be formally greater than R, and therefore the particle is not confined in the accelerator and the acceleration terminates at the instant of particle escape for $\varepsilon \leqslant qRB_\perp$, or (when $B_\perp \ll E_\perp$) the particle is not confined from the very beginning, and hence the energy gain is bounded by the difference of the electric potential across the acceleration region, i.e., $\varepsilon \leqslant qRE_{\rm eff} = \eta qRB$. In what follows, we neglect a factor ~ 1 and assume that $B = B_\perp$ and $E = E_\perp = E_{\rm eff} = \eta B$.

Therefore, the absolute upper bound for the particle energy is defined by either the acceleration – losses balance condition (1),

$$\varepsilon_{\rm max}^4 = \frac{3\,\eta B R^2}{2\,q}\,(mc^2)^4\,, \tag{4}$$

or condition (3), specifically, the lesser of these two values.

The total energy of the electromagnetic field in the spherical volume of radius R for an accelerator capable of generating cosmic rays with an energy $\varepsilon_{\rm max}$ is $W = R^3(B^2 + E^2)/6$, which gives

$$W > \frac{2}{27}\,\frac{q^2}{R}\left(\frac{\varepsilon_{\rm max}}{mc^2}\right)^8 \frac{1+\eta^2}{\eta^2} \tag{5}$$

for Eqn (4) and

$$W > \frac{R}{6}\left(\frac{\varepsilon_{\rm max}}{q}\right)^2 \tag{6}$$

for condition (3).

It is possible to minimize the requirements on the field energy in the accelerator by increasing R in relation (5) and decreasing it in relation (6). This implies the existence of the optimal size

$$R^{\rm (opt)} \approx \frac{2}{3}\,\frac{\sqrt{1+\eta^2}}{\eta}\,\frac{q^2\varepsilon_{\rm max}^3}{(mc^2)^4}\,, \tag{7}$$

which corresponds to the minimal possible accelerator energy content

$$W^{\rm (opt)} \approx \frac{1}{9}\,\frac{\sqrt{1+\eta^2}}{\eta}\,\frac{\varepsilon_{\rm max}^5}{(mc^2)^4} \tag{8}$$

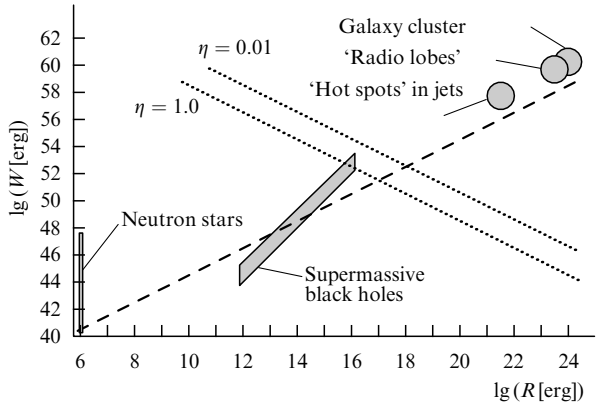

Figure 1. Minimal requirements on the energy content of a 10^{20} eV proton source for acceleration efficiencies $\eta = 1$ and $\eta = 10^{-2}$: expressions (5) (dotted lines) and (6) (dashed line) as functions of the acceleration region size.

and the optimal magnitude of the magnetic field

$$B^{\rm (opt)} \approx \frac{3}{2}\,\frac{\eta}{1+\eta^2}\,\frac{(mc^2)^4}{q^3\varepsilon_{\rm max}^2}\,, \tag{9}$$

with $E^{\rm (opt)} = \eta B^{\rm (opt)}$. The energy requirements defined by relations (5) and (6) are presented in Fig. 1. Also shown in Fig. 1 are the parameter ranges typical for neutron stars, rotating black holes with a near-Eddington accretion rate, galactic clusters, and those regions of jets in active galactic nuclei where the ejection velocities are no longer relativistic. Figure 1 shows two types of such regions: hot spots, i.e., bright objects of subkiloparsec size located at a distance ranging from several to dozens of kiloparsecs from the nucleus, and radio lobes — regions measuring several hundred kiloparsecs formed by a shock wave that delimits the jet substance and the intergalactic medium.

We estimate the optimal parameters for a source of protons with the energy $\varepsilon_{\rm max} = 10^{20}$ eV. The total energy of the electromagnetic field in the accelerator should be no less than $W^{\rm (opt)} \approx 3 \times 10^{51}$ erg, the optimal size is of the order of 10^{17} cm, and the optimal magnitude of the magnetic field is ~ 3 G. In these estimates, we assumed that $\eta = 1$ to relax the requirements on the field energy in the accelerator as much as possible. An even greater value of η (the electric field stronger than the magnetic one) does not lead to an appreciable lowering of $W^{\rm (opt)}$.

Naturally, the above results also apply to an accelerator that moves as a whole with a Lorentz factor $\Gamma \gg 1$; in this case, all quantities are measured in the comoving frame of reference. However, it is convenient to transform Eqns (7) – (9) such that $W^{\rm (opt)}$ and $\varepsilon_{\rm max}$ are measured in the laboratory frame of reference and $R^{\rm (opt)}$, $B^{\rm (opt)}$, and $E^{\rm (opt)}$ in the comoving frame of reference. We substitute $\varepsilon_{\rm max} = \Gamma\varepsilon'_{\rm max}$ to obtain

$$W_{\rm rel}^{\rm (opt)} = \frac{W^{\rm (opt)}}{\Gamma^4}\,, \tag{10}$$

$$R_{\rm rel}'^{\rm (opt)} = \frac{R^{\rm (opt)}}{\Gamma^3}\,, \tag{11}$$

$$B_{\rm rel}'^{\rm (opt)} = \Gamma^2 B^{\rm (opt)}\,, \tag{12}$$

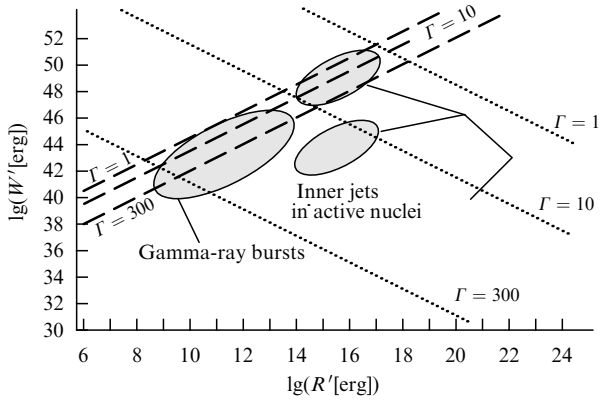

Figure 2. Minimal requirements on the energy content of a 10^{20} eV proton source as functions of the acceleration region size in the comoving frame of reference $R' = R/\gamma$. Expression (5), which scales as Γ^{-7}, is represented by dotted lines for an accelerator at rest and for Lorentz factors $\Gamma = 10$ and $\Gamma = 300$ ($\eta = 1$). Expression (6) is represented by dashed lines (scales as Γ^1). For inner jets in active galactic nuclei, the upper zone corresponds to hadronic gamma-ray radiation models and the lower zone to the leptonic ones.

where the quantities measured in the comoving frame of reference are primed.

The energy requirements represented by Eqns (10)–(12) are shown in Fig. 2. The parameter domains characteristic of the plasma flows in gamma-ray bursts ($\Gamma \sim 300$) and inner, relativistic ($\Gamma \sim 10$) jet regions in active galactic nuclei are indicated. Clearly, the acceleration of ultrahigh-energy cosmic rays in ultrarelativistic flows has the advantage of bringing the optimal size to a more 'comfortable' range, which is especially important for short-lived sources, for instance, gamma-ray bursts.

3. Converter acceleration mechanism

The most universal supplier of high-energy particles is the Fermi mechanism, and the acceleration is due to large-scale gradients in the hydrodynamic velocity of plasma. In particular, the acceleration in shear flows and collisionless shock waves has long been known [1, 3, 10]. As shown in Section 2, ion acceleration to ultrahigh energies is easier to ensure in ultrarelativistic flows.

While on the subject of the Fermi mechanism, the so-called stochastic acceleration is commonly implied. To estimate the suitability of this mechanism for the generation of ultrahigh-energy cosmic rays, we recall its scheme by the example of a shock wave. In a collisionless plasma, particles interact with each other via the magnetic field produced by the currents flowing through the plasma. The magnetic field is frozen into the plasma on both sides of the shock front, where the hydrodynamic plasma velocity experiences a jump; therefore, for a particle with a sufficiently long mean free path (i.e., with a sufficiently large momentum), the transit through the front is like a collision with a moving wall. The particles may either gain energy or lose it, depending on the direction of its motion, but on average the energy increases. This acceleration is similar to gas heating in a vessel with approaching walls, with the only difference that there is no second wall to reflect the particles back towards the shock front. Long-term acceleration and a substantial energy gain are possible only for the particles that can repeatedly cross the shock front in the opposite direction by overtaking it due to diffusive motion in the nonuniform magnetic field.

The average statistical particle acceleration rate in a nonrelativistic shock increases proportionally to the square of its velocity. The higher the velocity, the higher the maximum energy of accelerated particles. However, in a relativistic shock wave whose velocity is close to the speed of light, the acceleration mechanism considered above turns out to be inefficient. There are two reasons for this. First, the hydrodynamic velocity of the flow behind the front of a relativistic shock wave is equal to one third of the speed of light, and therefore the regular motion of particles prevails over their diffusive displacement and they have little chance to return to the front and continue their acceleration. Second, the plasma compression in the shock wave has the effect that the component of the frozen-in magnetic field parallel to the front increases, while the perpendicular component remains invariable. As a result, the particle drift velocity in the nonuniform magnetic field is directed approximately parallel to the front and the particles describe cycloids that do not cross the front. These theoretical considerations are borne out by numerical simulations [18, 19].

Efficient particle acceleration in relativistic shock waves and shear flows is nevertheless possible [5]. Paradoxically, the main role is here played by the interaction of accelerated particles with photon fields in accelerators, which is ordinarily regarded merely as an impediment, an additional channel of energy loss. Under certain conditions, collisions with photons may be treated as a mechanism of random 'activation' and 'deactivation' of the electric charge. The acceleration scheme described above is then modified as follows (Fig. 3). When traversing the shock front and experiencing reflections from the inhomogeneities of the magnetic field, a charged particle increases its energy to become neutral upon interacting with a photon, which allows it to traverse the front in the opposite direction unhindered by the magnetic field. On finding itself in front of the shock wave, the particle comes to be charged once again, such that the whole acceleration cycle is repeated over and over again. This particle acceleration mechanism may be termed the converter mechanism; calculations show that it plays a crucial role in the radiation and dynamics of relativistic flows [5, 6, 20].

Of course, the activation and deactivation of electric charge is no more than a conventional way of describing the processes occurring. For instance, we trace the chain of transformations beginning with the interaction of a proton with a high-energy gamma-ray photon. The photons whose energy exceeds 300 MeV in the rest frame of the proton can excite its internal (quark) degrees of freedom. The cross section of this process rapidly attains its peak $\sigma_\pi \approx 6 \times 10^{-28}$ cm^2 for the photon energy $\Delta_p \approx 340$ MeV (which may be considered the effective threshold of the reaction) and gradually decreases to $\approx 10^{-28}$ cm^2 for extremely energetic photons. The resultant excited hadron (typically, a Δ resonance) almost instantaneously decays into a nucleon and a pion:

$$\mathrm{p} + \gamma \to \Delta \to \mathrm{n} + \pi^+ \tag{13}$$

or

$$\mathrm{p} + \gamma \to \Delta \to \mathrm{p} + \pi^0 . \tag{14}$$

In approximately one-third of the cases, a charged pion forms and the proton transforms into a neutron. Neutrons have the

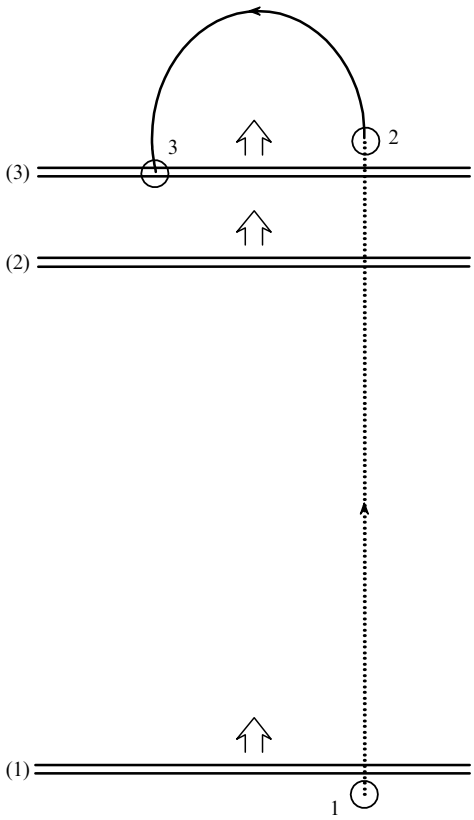

Figure 3. In the converter acceleration mechanism, a particle escapes from the shock wave being neutral (time instant 1) and travels rectilinearly until the moment it transforms to the charged one (time instant 2). During this time, the particle overtakes the shock front by some distance and therefore gains a sufficient store of time to start moving in the opposite direction in the magnetic field before it is entrained by the shock once again (time instant 3). The particle and shock front positions at the corresponding instants are numbered 1, 2, and 3.

same quark structure and interact with photons by the same scheme, i.e., transforming to protons. A by-product of the proton – neutron cycle is high-energy charged pions, whose decay gives rise to secondary electrons and positrons, as well as neutrino radiation.

A similar transformation chain also exists for electrons. It begins with photon scattering from a relativistic electron. As a result of the inverse Compton effect (comptonization), the photon energy upon scattering is many times higher, but for Thomson scattering, it amounts to only a small fraction of the electron energy. This interaction gradually takes energy from the electrons and does not favor their acceleration. However, the broadband radiation spectrum of cosmic accelerators also involves high-frequency photons scattered in the Klein – Nishina regime. In this case, the comptonized radiation spectrum has two peaks: with equal probabilities, an electron either retains the major part of its energy or transfers it to the photon. In the latter case, it can be said that the accelerated particle changes its charge, because the photon produced travels in the same direction as the initial electron and carries almost all of its energy. The high-energy comptonized photons interact with the relatively low-frequency background radiation to produce electron – positron pairs, the energy being approximately equally distributed between an electron and a positron. The transformation chain described above results in the closed cycle of activation and deactivation of accelerated particle charge. The fact that the number of accelerated particles doubles is of no fundamental importance. The converter acceleration of electrons and positrons has no direct bearing on the origination problem of ultrahigh-energy cosmic rays. We note, however, that the radiation of particles accelerated by this mechanism exhibits unique features (see Section 4): when recorded in the emission of some astrophysical object, they allow judging whether the converter mechanism operates in the object.

The small cross section of photopion reactions is the main limiting factor for the converter acceleration. The most favorable conditions for its realization exist in active galactic nuclei and gamma-ray bursts, where both ultrarelativistic matter flows in the form of jets and dense photon fields simultaneously exist (see review Refs [21, 22]).

The optical thickness τ that characterizes the accelerated-particle interaction with photons depends on the source geometry. For a continuous flow or a shock wave produced by a central compact object and propagating with an angular opening greater than $1/\Gamma$, we have

$$\tau \approx \frac{\sigma_\pi L(\varepsilon_*)\,\Theta^2}{4\,\pi R c \varepsilon_*}\,, \tag{15}$$

where L is the observed luminosity per logarithmic frequency interval for photons with energies in the vicinity of $\varepsilon_* = 2\,mc^2\Delta_\mathrm{p}/(\varepsilon\,\Theta^2)$, where the nucleon – photon interaction is most efficient, ε is the energy of the accelerated particle, R is the distance to the central object, Γ is the Lorentz factor of the relativistic flow, and m is the nucleon mass. The beam pattern of the photon source has the width $\Theta \sim 1/\Gamma$ for jets and $\Theta \sim 1$ for regions with broad emission lines in active galactic nuclei or for radiation scattered by the interstellar gas in the vicinity of gamma-ray bursts.

We give estimates for three qualitatively different cases. For internal jets in active galactic nuclei (with the inclusion of only the intrinsic radiation of the jet with $\Theta = 1/\Gamma$), where the observed luminosity $L(\varepsilon_*)$ per logarithmic frequency interval is implicitly dependent on the particle energy, we have

$$\tau \approx 10^{-1}\left(\frac{L(\varepsilon_*)}{10^{45}\,\mathrm{erg\,s^{-1}}}\right)\left(\frac{\varepsilon}{10^{18}\,\mathrm{eV}}\right)\left(\frac{10}{\Gamma}\right)^4\left(\frac{10^{15}\,\mathrm{cm}}{R}\right). \tag{16}$$

Radiation from regions with broad emission lines in active galactic nuclei produces the optical depth

$$\tau \sim 5\times 10^{-2}\left(\frac{L}{10^{44}\,\mathrm{erg\,s^{-1}}}\right)\left(\frac{10\,\mathrm{eV}}{\bar{\varepsilon}}\right)\left(\frac{10^{17}\,\mathrm{cm}}{R}\right), \tag{17}$$

which is independent of the particle energy: for all particles with energies $\varepsilon > 2\,mc^2\Delta_\mathrm{p}/\bar{\varepsilon} \approx 5\times 10^{16}$ eV, the number of effectively interacting photons is invariable due to their narrow spectral distribution (primarily in the vicinity of $\bar{\varepsilon} \sim 10$ eV). In gamma-ray bursts, the optical depth is

$$\tau \approx 3\times 10^{-3}\left(\frac{E(\varepsilon_*)}{10^{52}\,\mathrm{erg}}\right)\left(\frac{\varepsilon}{10^{16}\,\mathrm{eV}}\right)\left(\frac{100}{\Gamma}\right)^2\left(\frac{10^{16}\,\mathrm{cm}}{R}\right)^2. \tag{18}$$

Therefore, the conversion probability in every cycle is ordinarily much lower than unity. There are exceptions, for instance, at the base of a relativistic flow, where the optical thickness is large and conversion losses suppress acceleration. But as the distance from the jet base increases, acceleration

becomes possible once again and encompasses particles with a progressively higher energy as the radiation density decreases to the extent that the conversion probability in a single acceleration cycle becomes appreciably lower than unity. It is clear from the aforesaid that the converter acceleration is self-tunable.

We note that the neutron-to-proton conversion probability is always higher than

$$p_{\rm cn}^{(\min)} = \frac{Rmc}{t_{\rm n}\varepsilon} \approx 3\times 10^{-2}\left(\frac{10^{15}\,{\rm eV}}{\varepsilon}\right)\left(\frac{R}{10^{18}\,{\rm cm}}\right) \qquad (19)$$

owing to spontaneous neutron decay. Here, $t_{\rm n} \approx 900$ s is the free-neutron lifetime. The decay is important for low-energy particles, especially in the first acceleration cycle, whereas photopion reactions are more effective at high energies.

4. Features of the energy gain and radiation by particles during converter acceleration

The converter acceleration mechanism enables particles to attain the energy 10^{20} eV in only 2–4 passages through the shock front. For the standard diffusive acceleration, this would require many dozens of passages; the difficulties of realizing this mechanism are accordingly multiplied. This distinction may be explained as follows.

The velocity of particles that escape from the relativistic shock wave is, in the rest-frame system, directed almost parallel to the velocity of the shock wave. But the trajectory of charged particles immediately starts to bend under the action of a magnetic field. As soon as the angle between the particle velocity and the direction of the shock propagation attains a value of the order of the inverse Lorentz factor, the shock front catches up with the escaping particle and completes the acceleration cycle. The cycle result is that the particle energy increases twofold on average.

In the case of converter acceleration, a particle leaves the shock wave being neutral and travels rectilinearly until the instant of its transformation into a charged particle. During this time, the particle overtakes the shock front by some distance and hence acquires a sufficient time reserve to turn towards the shock wave in the magnetic field before it is entrained by the shock once again. Therefore, a converter acceleration cycle has the result that the particle energy increases not twofold but by about the factor γ^2, where γ is the Lorentz factor of the shock wave.

The probability that the particle converting from charged to neutral and backwards occurs in the right sequence and the particles interact with photons that have the appropriate energy is much lower than unity. On the other hand, the energy of a particle that goes through a complete acceleration cycle increases by a factor $g \sim \Gamma^2$, which ranges from several hundred for jets in active galactic nuclei to several hundred thousand for gamma-ray bursts. Upon experiencing several acceleration cycles, the initial quasimonoenergetic injected-particle distribution transforms into a saw-tooth distribution (Fig. 4). Its envelope may be approximately represented as a power-law function $\mathrm{d}N/\mathrm{d}\varepsilon \propto \varepsilon^{-\alpha}$ with the exponent

$$\alpha = 1 - \frac{\ln k}{\ln g}\,, \qquad (20)$$

which depends only slightly on the particle energy. When the cycle pass-through probability k times the energy gain factor g exceeds unity, the converter mechanism peaks in efficiency:

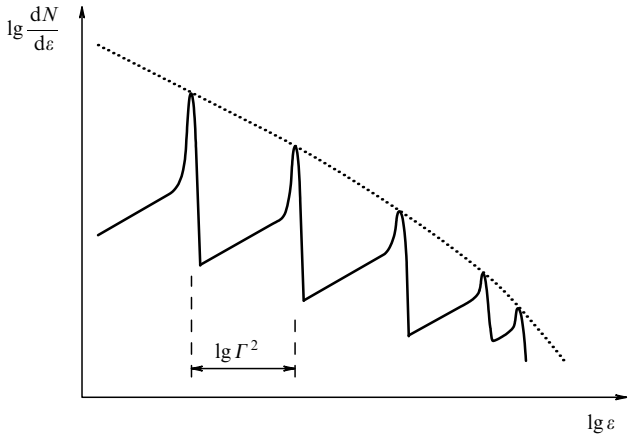

Figure 4. Schematic view of the particle distribution (solid line) resulting from the converter acceleration for a quasimonoenergetic injection. The dips in the spectrum persist as long as the width of the injection spectrum in logarithmic units is less than $\lg \Gamma^2$.

the total energy content in accelerated particles increases every cycle, the main contribution being due to particles whose energy is close to the maximum attainable energy.

The shock front can be crossed in the opposite direction only by the particles that manage not to lose energy (for instance, by synchrotron radiation) in the time required to complete a half-turn in the magnetic field behind the front. The particles that lose half of their energy during this turn are termed critical. In the diffusive acceleration, the particle energy increases approximately twofold in each cycle (except for the first one), and therefore the critical energy is also the highest attainable, whereby the energy loss rate is comparable to the acceleration rate.

Although the energy of particles escaping from the shock wave is bounded by the critical value, the energy of particles fed to the shock from the outside may be many times higher. Supercritical particles lose energy on traveling a distance many times shorter than their gyroradius, i.e., being deflected only slightly from the initial direction of their travel [almost strictly backwards in the frame of reference comoving with the matter behind the shock front (Fig. 5)]. Accordingly, the supercritical-particle radiation beam pattern is strongly elongated in the direction opposite to the shock velocity, as is the particle velocity distribution in the frame of reference of the jet [6]. Due to the relativistic aberration of light, a rest-frame observer nevertheless sees the beam pattern elongated in the direction of jet motion, but it turns out to be significantly broader than the beam pattern of the lower-frequency radiation of subcritical particles. Radiation of supercritical particles, which is primarily confined to the X- and gamma-ray ranges, may be observed at a large angle to the jet axis, i.e., it is off-axial (see Fig. 5).

The occurrence of off-axial radiation explains, for instance, the phenomenon of delayed hard radiation of gamma-ray bursts. The delay in this case is geometrical in nature: owing to the broadened radiation beam pattern, the off-axial emission is observed from a broader segment of a spherical shock wave, whose rim is more distant from the observer than its central part. The radiation beam pattern broadening may also account for detection of so-called unidentified sources of hard gamma-ray radiation (a large number of such sources were discovered by the EGRET

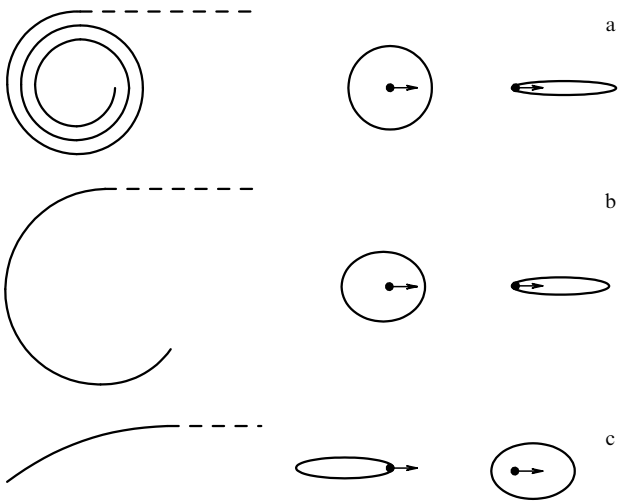

Figure 5. Variation of the radiation beam pattern in moving from subcritical (a) to critical (b) and then to supercritical (c) particle energy. The left part of the picture shows conventional particle trajectories during the radiation of half their energy, the central part shows typical radiation beam patterns in the comoving frame of reference, and the right part depicts typical radiation beam patterns in the laboratory frame of reference.

(Energetic Gamma Ray Experiment Telescope) space telescope in 1992 – 1994). These sources are supposedly related to those quasars whose jets are oriented at large angles to the line-of-sight direction and therefore do not produce appreciable radiation in lower-frequency ranges, where the jet emission is highly directional. High-energy neutrino emission of accompanying the decay of pions produced in inelastic proton – neutron collisions in relativistic jets may also have a broad beam pattern.

5. Conclusion

We have considered the fundamental bounds for the cosmic accelerator parameters. They indicate that the production of cosmic rays with energies ranging up to the highest reliably observed values is possible (at least theoretically) due to the action of the electromagnetic fields of astrophysical objects on the relatively low-energy ions present in these objects. There also exists an acceleration mechanism involving alternate conversion of protons to neutrons and back. This mechanism is operable in a broad class of sources with relativistic flows and is capable of transferring the power of these flows to $\sim 10^{20}$ eV cosmic rays with the efficiency approaching 100%. Therefore, it is possible to interpret all presently existing observations of ultrahigh-energy cosmic rays without invoking 'new physics,' i.e., using only reliably established physical laws and astrophysical facts.

Estimates show that different regions in the relativistic jets in active galactic nuclei, shock waves in galaxy clusters, and gamma-ray bursts may 'aspire' to play the role of accelerators for particles with an energy $\lesssim 10^{20}$ eV. With the exception of gamma-ray bursts, these all are galactic-scale objects. In particular, neutron stars and black holes, including the supermassive ones, cannot be the sources of cosmic rays.

Finally, we dwell on the validity range of the origination picture of ultrahigh-energy cosmic rays outlined in this report. The converter acceleration mechanism leads to a specific prediction about the particle composition of cosmic rays: these particles should be protons and nothing but protons. The existing data argue in favor of this proposition, although an unambiguous conclusion cannot be reached at the moment. If future observations reveal the presence of a substantial fraction of atomic nuclei in ultrahigh-energy cosmic rays, there will be no way of explaining their origin on the basis of the converter mechanism. But it is not inconceivable that there exists a different, and yet equally efficient, particle acceleration mechanism.

We have shown, however, that general electrodynamic considerations lead to a very strong dependence of the required field energy in an accelerator on the energy of the particles it produces, irrespective of the acceleration mechanism. For the known astrophysical objects, the acceleration limit for protons is therefore $(3-5) \times 10^{21}$ eV in the framework of the canonical model of cosmic ray generation. In this case, the list of potential sources is restricted to hot spots in the jets of active galactic nuclei, radio lobes, and galaxy clusters. In all these cases, the acceleration is limited by the particle escape, and attaining the specified energy value is possible only under rather speculative assumptions about large-scale magnetic field ordering and the high dimensionless acceleration rate $\eta \approx 1$. Heavy nuclei may be accelerated to even higher (Z times) energies, such that the acceleration scenario can formally account for the cosmic rays ranging up to 10^{23} eV in energy. At the same time, owing to the fragmentation of the nuclei (in the interaction with the photons of the microwave background radiation) their propagation distance is bounded by ~ 1 Mpc. Gamma bursts are the only sources in so close a neighborhood of our galaxy, and hence the highest cosmic ray energy observable on the earth cannot exceed the somewhat lower value $\sim 3 \times 10^{22}$ eV, which corresponds to the limit of acceleration in gamma-ray bursts for iron nuclei (for protons, this limit is $\sim 10^{21}$ eV).

This work was supported by the Russian Foundation for Basic Research (Project No. 05-02-17525), the Council of the President of the Russian Federation for Grants for the support of young Russian scientists and leading scientific schools of the Russian Federation (Grant No. NSh-4588.2006.2), and the Origin and Evolution of Stars and Galaxies Program of the Presidium of the Russian Academy of Sciences. The authors are grateful to V S Ptuskin for giving them the opportunity to familiarize themselves with his paper [3] prior to its publication.

References

1. Ginzburg V L *Usp. Fiz. Nauk* **166** 169 (1996) [*Phys. Usp.* **39** 155 (1996)]
2. Berezinskii V S et al. *Astrofizika Kosmicheskikh Luchei* (Astrophysics of Cosmic Rays) (Ed.) V L Ginzburg 2nd ed. (Moscow: Nauka, 1990)
3. Ptuskin V S *Usp. Fiz. Nauk* **177** (5) (2007) [*Phys. Usp.* **50** (5) (2007)]
4. Aharonian F A et al. *Phys. Rev. D* **66** 023005 (2002)
5. Derishev E V et al. *Phys. Rev. D* **68** 043003 (2003)
6. Derishev E V, Aharonian F A, Kocharovsky Vl V *Astrophys. J.* **655** 980 (2007)
7. Nagano M, Watson A A *Rev. Mod. Phys.* **72** 689 (2000)
8. Hillas A M, in *Cosmology, Galaxy Formation and Astroparticle Physics, Oxford, UK, 2006* (Eds H-R Klockner et al.) (in press); astro-ph/0607109
9. Zatsepin G T, Kuz'min V A *Pis'ma Zh. Eksp. Teor. Fiz.* **4** 114 (1966) [*JETP Lett.* **4** 78 (1966)]
10. Greisen K *Phys. Rev. Lett.* **16** 748 (1966)
11. Berezinsky V *Nucl. Phys. B: Proc. Suppl.* **81** 311 (2000)
12. Fermi E *Phys. Rev.* **75** 1169 (1949)

13. Ginzburg V L, Syrovatskii S I *Proiskhozhdenie Kosmicheskikh Luchei* (The Origin of Cosmic Rays) (Moscow: Izd. AN SSSR, 1963) [Translated into English (Oxford: Pergamon Press, 1964)]
14. Krymskii G F *Dokl. Akad. Nauk SSSR* **234** 1306 (1977) [*Sov. Phys. Dokl.* **22** 327 (1977)]
15. Bell A R *Mon. Not. R. Astron. Soc.* **182** 147 (1978)
16. Malkov M A, Drury L O'C *Rep. Prog. Phys.* **64** 429 (2001)
17. Aharonian F et al. *Astron. Astrophys.* **448** L43 (2006)
18. Niemiec J, Ostrowski M *Astrophys. J.* **641** 984 (2006)
19. Lemoine M, Pelletier G, Benoit R *Astrophys. J.* **645** L129 (2006)
20. Stern B E *Mon. Not. R. Astron. Soc.* **345** 590 (2003)
21. Urry C M, Padovani P *Publ. Astron. Soc. Pacific* **107** 803 (1995)
22. Mészáros P *Annu. Rev. Astron. Astrophys.* **40** 137 (2002)

PACS numbers: 41.20.Jb, 52.35.Mw, **94.20.–y**

DOI: 10.1070/PU2007v050n03ABEH006282

Modification of the earth's ionosphere by high-power high-frequency radio waves

V L Frolov, N V Bakhmet'eva, V V Belikovich, G G Vertogradov, V G Vertogradov, G P Komrakov, D S Kotik, N A Mityakov, S V Polyakov, V O Rapoport, E N Sergeev, E D Tereshchenko, A V Tolmacheva, V P Uryadov, B Z Khudukon

1. Introduction

The ionosphere, being the upper part of the terrestrial atmosphere, has a decisive effect on both the nature of vital functions on Earth and the properties of different tele- and radio communication channels. In this connection, it has attracted the close attention of researchers already for many decades. The range of ionospheric research is extremely wide and embraces problems such as the physics of plasma formation, plasma dynamics and the mechanisms of plasma turbulization, ionospheric chemistry, and the propagation of radio waves in different ranges. The capabilities of conventional methods of ionospheric research were greatly enhanced when active ionospheric experiments were started. These include plasma modification by high-power radio wave beams produced by ground-based and space-borne high-frequency (HF) radio transmitters, as well as the injection of charged particle beams and chemical reagents from aboard artificial earth satellites (AESs) and geophysical rockets. The success achieved in active experiments allowed considering the ionosphere as a natural space laboratory for modeling different processes occurring in plasmas [1]. The relatively high stability and the practically infinite volume of the ionospheric plasma, as well as the variation over a wide range in its possible parameter values, permit a broad class of currently topical problems to be solved on an experimental basis.

The variation in ionospheric properties in the field of high-power radio waves was first encountered over 70 years ago in connection with the discovery of the Luxemburg–Gorky effect in 1933 [2]. The decisive roles in the theoretical interpretation of this effect were played by Ginzburg, Gurevich, and Vilenskii. The explanation of the Luxemburg–Gorky effect led to the understanding of the role of the nonlinear properties of ionospheric plasma, which show up under heating by a high-power radio wave and were considered at length by Ginzburg and Gurevich in Ref. [3]. The investigations conducted lent impetus to the construction of special-purpose high-power heater facilities for the modification of the ionosphere. In the USSR, the first facility was put into operation in the Scientific Research Radio Institute (Moscow) in 1961. More recently, constructed in the USA were the facilities Boulder in 1970 and Arecibo in 1971. At the Radiophysical Research Institute (NIRFI), this line of investigation was initiated by Getmantsev. Under his supervision, the Zimenki facility was constructed in 1973 near Nizhnii Novgorod (formerly the city of Gorky). In 1976, the Polar Geophysical Institute (PGI) of the Kola Branch of the USSR Academy of Sciences succeeded in its efforts to construct the Monchegorsk facility in polar latitudes near Murmansk.

Already in the first experiments on ionospheric modification by high-power radio waves carried out in the 1960s–1970s, apart from the expected large-scale variations in plasma temperature and density, several new phenomena related to the generation of artificial plasma oscillations and artificial plasma density irregularities with scale lengths ranging from fractions of a meter to several kilometers transversely to the geomagnetic field were discovered [4, 5], the Getmantsev effect was discovered [6], and the formation of artificial periodic irregularities of ionospheric plasma density in the field of a high-power standing radio wave was experimentally borne out [7]. There emerged a new line of research, which soon became one of high-priority areas in radiophysics and found diversified uses in geophysics, plasma physics, and space physics. An important point is that modifying the ionosphere by high-power radio waves does not pollute the environment and has no undesirable ecological consequences, because this action on the ionosphere is negligible in power in comparison with natural actions. At the same time, the possibility exists of conducting repeated measurements of the characteristics of the upper terrestrial atmosphere on a regular basis by using the thoroughly elaborated radiophysical techniques for the remote diagnostics of artificially produced plasma perturbations.

The results achieved fostered the construction of new, more powerful heaters in northern Norway (Tromsø, 1980) and in the USSR (Sura, 1981). More recently, in the 1990s, a start was made on the construction of a facility in Alaska (USA) in the framework of the High Frequency Active Auroral Research Program (HAARP); its first stage was put into service in the late 1990s. To this day, efforts are directed towards upgrading the potentialities of the facility. Among other facilities constructed in the 1980s–1990s are Gissar (Tadjikistan, 1981), a facility near Kharkov (Ukraine, 1987), and the High Power Auroral Simulation (HIPAS) facility (USA, 1990). Today, experiments in the modification of the ionosphere are conducted primarily at three facilities: HAARP and Tromsø in polar latitudes and Sura in middle latitudes. The remaining facilities either have fallen apart or are no longer in active use. In recent years, the British have undertaken the construction of the SPEAR (Space Plasma Exploration by Active Radar) facility on the island of Spitsbergen, in the polar cap zone. In 2004, the first stage of SPEAR was put into operation and heater experiments were started.

In this report, we briefly outline the results of experiments in artificial influence on the ionosphere by high-power HF

radiation from ground-based transmitters. They were performed at NIRFI in cooperation with many Russian and foreign institutions and include investigations of the properties of artificial ionospheric turbulence (AIT), of the generation of combination-frequency signals by an ionospheric source in the very low frequency (VLF), superlow frequency (SLF), and ultralow frequency (ULF) ranges, and of different ionospheric layers with the help of artificial periodic irregularities. These investigations commenced at the Zimenki facility and continued at the Sura facility.

The Sura facility (NIRFI), which has received the status of a unique Russian facility (registration No. 06-30), comprises three high-frequency PKV-250 transmitters with the cw output power 3×250 kW in the 4 – 25 MHz frequency range. Each transmitter is loaded on its own antenna array with a 4.3 – 9.5 MHz frequency band. The three facility modules can work independently and emit a wave with ordinary or extraordinary polarization at its frequency, in its own timing, with the pulse duration ranging from 50 μs up to the cw output. In the regime of coherent radiation by all three heater modules (in this case, the total dimension of the antenna field is 300 by 300 m), the maximum effective output power is 80 – 280 MW, increasing with the frequency of the radiated wave. The heater beam can be deflected in the range $\pm 40^\circ$ from the vertical in the plane of the geomagnetic meridian. Different diagnostic facilities are deployed around the Sura heater, which fulfill the function of probing the ionosphere and detecting plasma perturbations induced by a high-power radio wave.

2. Artificial ionospheric turbulence

The interaction between a powerful HF radio wave with ordinary polarization and a plasma is accompanied by the excitation of AIT of different types, which is determined by the development of several nonlinear effects: (1) the generation of high-frequency (different plasma oscillations and waves) and low-frequency (first and foremost, plasma temperature and density irregularities with different scale lengths) plasma turbulence; (2) modification of the plasma density profile under the action of striction and thermal pressure forces, which results in the formation of focusing (in the F_2 region) and defocusing (in the E and F_1 regions) lenses, as well as of artificial periodic irregularities under the action of a high-power standing radio wave; (3) electron acceleration to suprathermal energies, which leads to additional plasma ionization and the glow of neutral gas in the optical and decimeter wavelength ranges; (4) the generation of secondary electromagnetic radiation (in particular, artificial radio-frequency ionospheric radiation); (5) the excitation of electric and magnetic fluctuation fields, etc. It is significant that the wide-ranging experimental and theoretical investigations performed during the last three decades, which are summarized in several dedicated journal issues [4, 8 – 13], have enabled a detailed study of the features of high-power wave interaction with different ionospheric plasma regions, an investigation of the production features and properties of AIT, and an elaboration of new methods for diagnosing the processes occurring in magnetoactive plasmas.

In Sections 2.1 – 2.4, we briefly formulate the main properties of AIT excited by a high-power radio wave of ordinary polarization in its reflection from the F_2 ionospheric region.

2.1 Development stages of the interaction between high-power radio-frequency radiation and plasma

Four stages may be distinguished in the development of the interaction of a high-power radio o-wave and the plasma of the F_2 ionospheric region [14]. During the first stage, which lasts 5 – 20 ms from the onset of the action and is characterized by a 10 – 20 dB intensity lowering of the signal of the pump wave (PW) reflected from the ionosphere, a striction parametric instability [15] develops near the level of reflection of the high-power radio wave, resulting in the generation of Langmuir plasma turbulence and electron acceleration to suprathermal energies. At the second stage, which lasts 0.5 – 3 s (up to the onset of the development of the anomalous attenuation effect), the signal of the reflected PW is observed to regain its intensity level, which is accompanied by the emergence of its characteristic quasiperiodic oscillations. So far, this effect has not been adequately explained. At the third stage, 0.5 – 10 s after the onset of the PW, the generation of upper-hybrid plasma turbulence and small-scale field-aligned ionospheric irregularities (SFAIIs) of size $l_\perp \leqslant 30 - 50$ m in the direction orthogonal to the terrestrial magnetic field is observed due to the development of a thermal (resonance) parametric instability [16, 17]. The scattering of the high-power radio wave from the SFAIIs leads to its anomalous attenuation (AA) — a lowering of the signal reflected from the ionosphere by 10 – 30 dB. The fourth stage, which sets in 10 – 30 s after the PW engagement, is characterized by the development of a self-focusing instability of the high-power radio wave [17, 18]. This leads to an increase in medium-scale ($l_\perp \approx 0.1 - 1$ km) field-aligned ionospheric irregularities (FAIIs), which are responsible for strong fluctuations in the radio waves reflected from the perturbed region of the ionosphere and for the formation of spreading F_{spread} on the ionograms for the traces of probing transmitter signals reflected from the ionosphere, which is characteristic of radio wave propagation through a turbulent medium. The generation of larger-scale irregularities with $l_\perp \geqslant 1 - 2$ km is attributed to the intensification of natural plasma density irregularities.

The ionosphere modification effects are markedly intensified when the conditions are fulfilled for the propagation of a high-power radio wave beam along the magnetic field in the region of resonance PW – plasma interaction (the 'magnetic zenith' effect) [19]. In this case, as a result of PW self-focusing by the irregularities elongating along the geomagnetic terrestrial field, which measure several hundred meters in the direction transverse to the geomagnetic field and which are filled with SFAIIs with $l_\perp \approx 1 - 10$ m, a strong local plasma heating occurs due to the anomalous absorption of the energy of the high-power ordinary radio wave in its scattering by the SFAIIs into upper-hybrid plasma waves. This leads to the formation of caverns, such that the high-power radio-frequency radiation flux splits into narrow beams and is confined to these caverns.

2.2 Dynamic and spectral characteristics of artificial ionospheric irregularities

The development times τ_{dev} of the FAIIs with $l_\perp \approx 1 - 10^3$ m depend strongly on their scale length (as $l_\perp^{0.5}$), the PW power (as P_{eff}^{-1}), and its schedule (via aftereffects), as well as the ionospheric conditions [14]. On average, $\tau_{\text{dev}} \approx 2 - 5$ s for $l_\perp \approx 10$ m and $P_{\text{eff}} \approx 20$ MW. The FAII relaxation times τ_{rel} are determined by the irregularity scale length $l_\perp$ [14]: a quadratic dependence $\tau_{\text{rel}}(l_\perp) \propto l_\perp^2$ occurs for $l_\perp \leqslant l_\perp^*$, a

weaker dependence $\tau_{\rm rel}(l_\perp) \propto l_\perp^{0.5}$ occurs for $l_\perp \geqslant l_\perp^*$ ($l_\perp^* \approx 3-20$ m is some characteristic irregularity scale length, the quantity $l_\perp^*$ decreases in moving from daytime to nighttime observation conditions). It is believed that the SFAII relaxation in the domain of the quadratic $\tau_{\rm rel}(l_\perp)$ dependence is due to the transverse ambipolar diffusion and is caused by longitudinal ambipolar plasma diffusion for $l_\perp > l_\perp^*$. The specific irregularity relaxation times also depend on the hour of the day, the PW reflection altitude $h_{\rm refl}$, the location of the irregularities inside the disturbed region, the PW radiation regime, the degree of ionospheric perturbation, etc. For $l_\perp \approx 10$ m and $h_{\rm refl} \approx 240$ km, the relaxation times in quiet geomagnetic conditions are 5 – 10 s in the daytime and lengthen to 15 – 20 s in the evening and to 20 – 40 s in the nighttime.

On the basis of cross section measurement data for the aspect scattering of radio waves in the high-frequency and very-high-frequency (VHF) ranges by anisotropic SFAIIs and measurements of AES signal flicker in radio wave transit through the disturbed region of the ionosphere, it was possible to measure the plasma density fluctuation spectrum in the $l_\perp \approx 1-4 \times 10^3$ m scale length range [14, 20, 21]. For a piece-wise power-law approximation of the dependence $\Phi_N(l_\perp) \propto l_\perp^p$, it was determined that $p \approx 4-5$ for $l_\perp \approx 1-3$ m, $p \sim 2-3$ for $l_\perp \approx 3-20$ m, $p \sim -(0.5-1)$ for $l_\perp \approx 50-200$ m, $p \sim 3$ for $l_\perp \approx 200-400$ m, $p \sim 1.5-2$ for $l_\perp \approx 600-800$ m, and $p \sim 3-4$ for $l_\perp \approx 0.8-4$ km. The peak of $\Phi_N(l_\perp)$ for scale lengths $l_\perp \approx 50$ m, which are close to the free-space wavelength of the high-power wave, is caused by the irregularity generation mechanism due to the development of a thermal (resonance) parametric instability. The second peak, which was observed for scale lengths $l_\perp \approx 400-600$ m, is attributable to the manifestation of the PW self-focusing instability in the plasma. On average, the characteristic magnitudes of the relative plasma density fluctuations at the stationary AIT development stage are $\delta N \approx 5\times10^{-3}-10^{-2}$ for $l_\perp \approx 1-2$ km, $\delta N \sim 10^{-3}-2\times10^{-3}$ for $l_\perp \approx 200-600$ m, and $\delta N \sim 5\times10^{-4}-10^{-3}$ for $l_\perp \approx 3-30$ m. During the first several seconds after PW engagement, owing to the faster growth of the irregularities with $l_\perp \approx 1-3$ m, the SAIT spectrum is inverted in form, peaking for scale lengths $l_\perp \approx 2-3$ m [14]. Measurements performed for different tilt angles of the high-power radio wave beam in the plane of the geomagnetic meridian enabled determining that SAITs are most intensively generated for tilt angles $\sim 12^\circ - 16^\circ$ south of the vertical [21].

Therefore, by varying the power, frequency, polarization, and schedule of the PW radiation, it is possible to control the spectral FAII characteristics, which is important for the use of AIT in solving research and applied problems [22].

Doppler measurements of the spectrum of HF and VHF radio waves scattered by SAIT permit obtaining information about the motion of scattering irregularities inside the perturbed ionospheric region. On the basis of the measurements of the Doppler spectra of the scattered signals, it was determined in Ref. [23] that radial SAIT motions from the center of the perturbed ionospheric region to its periphery are induced during its heating. Furthermore, this method allows studying the characteristics of moving ionospheric perturbations [24] and local geomagnetic pulsations [25] as well as measuring the electric field strength in the F_2 ionospheric region [26]. The authors of Refs [27, 28] investigated the effect of broadening of the Doppler spectrum of the scattered signal in conditions where the PW frequency is of the order of or slightly higher than a gyroresonance harmonic frequency in the PW — plasma interaction region. This may be an indication that a significant role in the processes of determining the dynamics of decametric SAITs is played by the electron Bernstein plasma oscillations driven by a high-power radio wave.

2.3 Artificial ionospheric radio-frequency radiation

It the more than 30 years since the discovery of stimulated electromagnetic emission (SEE) in the ionosphere [29, 30], intensive investigations of its properties have been pursued. This radiation emerges due to all kinds of interactions of electromagnetic waves and high-frequency plasma oscillations with low-frequency plasma turbulence whose production and evolution are governed by SFAIIs. The interplay and interference of different plasma processes in the generation of SEE in magnetoactive plasma underlie its broad diagnostic potential for studying the properties of both artificial and natural plasma turbulence. More than 15 SEE components are presently known; their comprehensive description is given in review Ref. [31]. Among its components whose spectral and dynamic characteristics have been studied in greatest detail are

(1) the main SEE spectral maximum, or down-shifted maximum (DM);

(2) broadband down-shifted radiation, or broad continuum (BC);

(3) the up-shifted maximum (UM);

(4) the broad up-shifted maximum (BUM). The generation of this maximum is observed when the PW frequency is close to or slightly higher than the frequency of a gyroresonance harmonic in the region of the interaction between the high-power radio wave and the plasma (under the conditions of measurements performed at the Sura facility, the electron gyrofrequency is $f_{\rm ce} \approx 1.3-1.35$ MHz);

(5) the striction narrow-band radiation component, or the ponderomotive narrow continuum (NC_p), observed at the development stage of a striction parametric instability;

(6) the thermal narrow continuum ($NC_{\rm th}$) observed at the development stage of a thermal (resonance) parametric instability;

(7) the BUM-like broad up-shifted structure (BUS), which shows up in the frequency ranges between the gyroharmonics.

The generation of different components in the SEE spectrum depends heavily on the frequency and power of the PW, as well as on the ionospheric conditions. The investigations carried out at the Sura facility [32] in its entire frequency range 4.3 – 9.5 MHz showed (Fig. 1) that (i) the shape of the SEE spectrum changes radically in a narrow range of PW frequencies, when $f_{\rm BH} \approx nf_{\rm ce}$, where n is the gyroharmonic number; (ii) the radiation is most intense in the frequency range between the fourth and fifth gyroharmonics; and (iii) the effect of gyroresonances also manifests itself outside the regions where $f_{\rm BH} \approx nf_{\rm ce}$.

Methods for diagnosing the high- and low-frequency turbulence were developed on the basis of SEE, which enabled carrying out measurements of the characteristic buildup and relaxation times of the Langmuir and upper-hybrid plasma waves [33], studying the SFAII effect on the generation of different SEE components [34], and investigating the effects observed in the nonlinear interaction of two high-power radio waves in a magnetoactive plasma [35]. The diagnostic SEE method was employed to study the transport properties in the upper ionosphere [36]. The characteristic

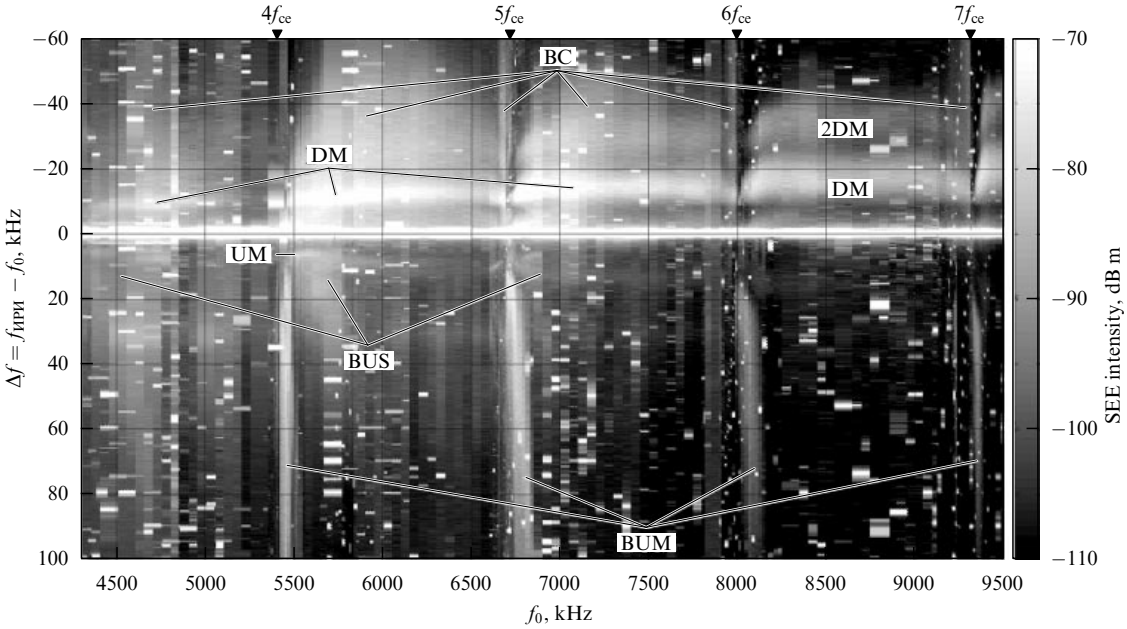

Figure 1. Dependence of the spectral SEE structure on the pump wave frequency in the 4.3 – 9.5 MHz range.

velocities $V_{||}$ of the plasma perturbation propagation along the geomagnetic field were found to be of the order of or appreciably higher than the electron thermal velocity $V_{Te} \approx 2 \times 10^7$ cm s^{-1} under the typical conditions of our experiments conducted in the F_2 ionospheric layer. This may testify to the importance of inclusion of thermal- and accelerated-electron fluxes, as well as of short-circuit currents through the background plasma in the mechanisms of AIT generation outside the regions of resonance high-power wave – plasma interaction [36 – 38].

In recent years, the generation of artificial radio-frequency radiation in the decimetric wavelength range (at frequencies ~ 600 MHz) [39] has been revealed. It is assumed that the SEE emerges in this case in the electron transitions between the high Rydberg levels of the molecules of neutral ionospheric plasma components excited by accelerated electrons.

2.4 Spatial structure of the perturbed ionospheric region

Measurements of the spatial structure of the perturbed ionospheric region above the Sura facility using the satellite radio tomography technique were first performed in August 2002 [40] and repeated in August 2005. Figure 2 shows the tomograms obtained in the evening (Figs 2a and 2b) and night (Figs 2c and 2d) observation hours, when the PW was reflected near the maximum of the F_2 ionospheric layer at altitudes $\sim 270 - 300$ km. Shown are the tomograms for both the plasma density (Figs 2a, 2c) and the difference reconstruction (Figs 2b, 2d), which demonstrates the fluctuations of the plasma density with regard to its average value. The experimental data were processed with the use of the Bayes probabilistic approach to ray (phase) tomography relying on the theory of stochastic inversion [41].

It is easy to see from Fig. 2 that the plasma density perturbations exhibit a strongly pronounced orientation along the geomagnetic field lines, are observed throughout the altitude range possible under the given geometry of the experiment, from ~ 200 km to $\sim 600 - 700$km, and are excited in a broader horizontal region (± 200 km relative to the center of the high-power radio wave beam) than the ionospheric region irradiated by the main lobe of the heater antenna directivity ($\sim 60 - 100$ km). The radiation pattern of the main antenna lobe of the heater is shown by dashed lines, and the direction of the geomagnetic field for the Sura facility location is shown with a solid line. From the tomograms presented it is also clear that cavities with a strong (up to 20%) plasma depletion develop in the southern sector of the antenna pattern of the heater. With the use of heating by oblique high-power radio wave beams it was determined that such structures are most efficiently produced when the radiation direction of the high-power radio wave in the ionosphere is close to the direction of geomagnetic field lines and are a manifestation of the 'magnetic zenith' effect [19]. It was also determined that the plasma density irregularities with $l_\perp \approx 100 - 1000$ m, which are responsible for the scintillation of a signal transmitted through the perturbed ionospheric region, are confined primarily within the large-scale regions with a strong decrease in the plasma density.

Our attention is caught by the occurrence of regions with a pronounced wave-like form of plasma density perturbation, which appear at the altitude of PW reflection and extend upwards along the geomagnetic field to altitudes $\sim 500 - 600$ km. Referring to Fig. 2, these perturbations are confined to narrow geomagnetic field tubes with transverse dimensions ~ 30 km and their typical scale lengths along the field direction are ~ 75 km for the evening ionosphere and ~ 55 km for the night one. The nature underlying the formation of these perturbations is still unclear.

Modification under daytime ionospheric conditions, when the PW is reflected at altitudes $\sim 200 - 220$ km, does not give rise to regions with strong plasma depletion; the plasma density perturbations are smaller in magnitude and longer ($\geqslant 50 - 100$ km) in scale lengths than at nighttime. The aforementioned wave-like structures extended along the geomagnetic field are not observed at these altitudes, either.

In 2005, the investigation of plasma perturbations induced by the Sura heater at altitudes ~ 710 km began at

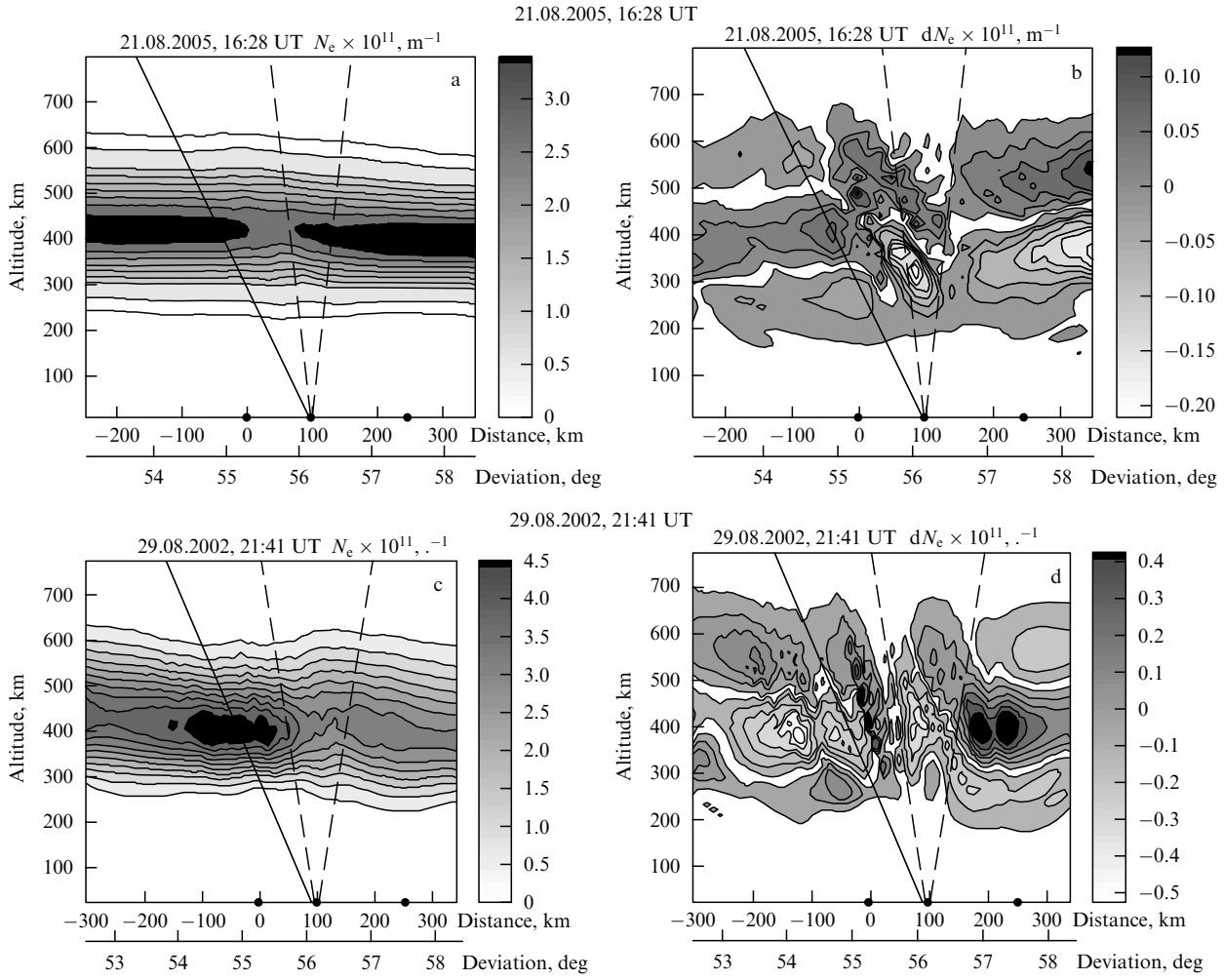

Figure 2. Tomographic reconstruction of the plasma density profile (a, c) and the density variations (b, d) in evening ionospheric conditions (a, b) and night ionospheric conditions (c, d).

NIRFI. The investigations were conducted with the help of the French microsatellite DEMETER (named from the 'Detection of Electromagnetic Emissions Transmitted from Earthquake Regions'), which has a unique set of instruments enabling measurements of different plasma perturbation parameters. The first measurements performed in the framework of the Sura – DEMETER program in the heating of the nighttime F_2 ionospheric region by an unmodulated PW, reflected near the maximum of the F_2 ionospheric layer, allowed the following conclusions [42]:

(i) strong (up to 5 – 10%) artificial fluctuations in the electron temperature (T_e) and density (N_e) and in the ion density (N_i) are observed at the altitude $\sim$ 710 km; variations in the ion temperature (T_i) are within the natural background fluctuation level of 1 – 2 %;

(ii) artificial fluctuations in T_e, N_e, and N_i are recorded at distances up to 400 km from the center of the perturbed geomagnetic tube that rests on the ionospheric region illuminated by a high-power radio-wave beam;

(iii) the excitation of electric field oscillations at frequencies $f \leqslant 1$ kHz is observed in the central part of the perturbed geomagnetic tube.

It is easily seen that on the whole, there is good agreement between plasma density variations measured by radio tomographic and satellite techniques.

In concluding this section, we note that despite the wealth of investigations made into AIT properties, several basic problems remain unexplored. In particular, the absence of adequate theoretical models of the generation of different SEE components hinders the development of SEE-based techniques for the diagnostics of natural and artificial plasma turbulence. It remains to elucidate the reasons underlying the generation of AIT far beyond the limits of the central part of the perturbed region, which sees the development of striction and thermal (resonance) parametric instabilities and intense plasma heating. The problems related to the nature of drift and wave-like motions induced by high-power radio waves in the perturbed ionospheric region also invite further investigation. Different manifestations of the effect of electrons accelerated by plasma turbulence on the high-power radio-wave — plasma interaction dynamics and the generation of different AIT components must be studied further.

In this report, we did not set ourselves the task of outlining the results of investigations into control of the propagation channel for HF and VHF radio waves via their refraction in large-scale FAIIs or scattering from SFAIIs. These investigations make up a separate important field of experiments carried out at the Sura heater; a substantial fraction of this field pertains to the study of the mechanisms of long-distance

propagation of HF waves under controllable conditions. We only note that Uryadov et al. [46] experimentally demonstrated the feasibility of controlling the long-distance propagation of HF waves via extraction of waveguide modes from the ionospheric channel due to aspect scattering from SFAIIs. In Ref. [26], a sporadic E layer was shown to have a pronounced effect on the emergence of signals with a frequency exceeding the highest applicable frequency (HAF) of the F region, when their extraction to the terrestrial surface may be effected by aspect scattering from the SFAIIs. The Sura — HAARP experiment, performed under Grant No. RPO-1334-NO-02 from the Civilian Research and Development Foundation (USA) in 2006, was an important milestone in the pursuance of research in this area. For HF waves, the path of their long-distance propagation controllable on both ends was created in this experiment. The waveguide modes of the ionospheric waveguide path were excited in the radiowave scattering from the SFAIIs induced in the ionosphere by HAARP radiation, and the path modes were extracted by their aspect scattering from the SFAIIs induced by the Sura heater [44]. The existence of this path opens up new possibilities for investigating the properties of channel radio wave propagation.

3. Progress in the investigation of the effect of low-frequency radio-wave generation in the ionosphere under the action of high-power modulated short-wave radio-frequency radiation

From the outset of research at the relatively low-power Zimenki heater (transmitter output 100 kW), the head of research Getmantsev took on the task of discovering the effect of low-frequency radio-wave generation in the ionosphere irradiated by modulated high-power HF radio waves. The formulation of this problem was based on the theory of nonlinear phenomena in plasma developed by Ginzburg and Gurevich [3] back in the 1950s. According to this theory, irradiation of the ionospheric plasma by an electromagnetic signal containing two carrier frequencies in its spectrum must lead to signals at the combination frequencies $f_1 \pm f_2$. Upon several attempts, the effect of combination-frequency signal (CFS) generation was discovered at the frequency $\Omega = f_1 - f_2$ [6, 45]. Closer investigation of CFS properties (spectral and polarization measurements and determination of the altitude of the low-frequency radiation source) led to an unambiguous conclusion about the nature of this radio-frequency radiation. It was determined that the mechanism of the observed CFS generation was directly related to the modulation of quasistationary ionospheric currents constantly present in the ionosphere at dynamo-region altitudes ($\approx 70-130$ km, the site of the strongest ionospheric currents) [46, 47]. In 1981, the discovery was registered as 'The phenomenon of electromagnetic wave generation by ionospheric currents under irradiation of the ionosphere by modulated short-wave radio-frequency radiation.' The effect discovered has come to be known as the Getmantsev effect [48]. For modern heater capabilities ($P_{\text{eff}} \approx 100-300$ MW) and the diagnostic techniques developed, low-frequency radiation is detected not only in the VLF range at the frequencies 0.5 – 10 kHz but also in the geomagnetic pulsation range at frequencies $\leqslant 10$ Hz.

Putting the Sura heater (the total output power of HF heater transmitters is $P = 750$ kW) into operation in 1981 opened up the possibility of carrying out research on a qualitatively new level, because the level of the ionospheric signal increased several-fold. This allowed more carefully verifying the propositions of the CFS generation theory, which had been developed by that time [49, 50]. Furthermore, two transmitters (with the total power $P = 200$ kW) were additionally constructed on the basis of the Sura heater in 1985 specifically for the pursuance of research into lower ionospheric effects. The transmitters were loaded on an 8-element antenna array for the zenith radiation of circularly polarized waves at a frequency close to the gyrofrequency of ionospheric electrons. This afforded a higher-efficiency ohmic plasma heating and substantially broadened the possibilities of the research conducted. The results of experiments performed on the Sura facility and their comparison with theoretical notions are summarized in review Ref. [51].

The experiments carried out at the Zimenki and Sura facilities enabled studies of

- the spectral characteristics of the CFS;
- the daily CFS variation and its dependence on the frequency, polarization, and power of the PW;
- polarization CFS characteristics;
- the fine structure of ionospheric currents;
- dependence of the low-frequency signal parameters on the source altitude.

To date, the methods of receiving and processing CFSs have been adequately elaborated, and the optimal conditions for their generation have been found. This allows using the Getmantsev effect for the diagnostics of the parameters of the lower ionosphere (the dynamo region) and the magnetosphere, as well as for deep probing of the earth's core. In this case, it is possible to gain information about

- the electric fields and currents in the terrestrial ionosphere and magnetosphere;
- the waveguide and resonance properties of the ionosphere and the conditions of low-frequency radiation propagation through the earth — ionosphere waveguide, radiation transmission through the ionosphere, and its propagation in the terrestrial magnetosphere;
- the characteristics of low-frequency wave interaction with energetic protons in terrestrial radiation belts;
- the effect of seismic activity and internal gravitational waves on the dynamics of the upper atmosphere;
- the distribution of the terrestrial surface conductivity with depth, which yields information about its geological structure.

Using the possibilities for the spatial control of a high-power radio wave beam furnished by the Sura heater, an investigation was made of a new type of ionospheric source, a traveling-wave antenna in the range of several kilohertz, and a study was made of the radiation pattern of the traveling ionospheric source [52]. This is, in essence, the Vavilov – Cherenkov radiation of a superluminal 'light spot' produced in the ionosphere by the tilting antenna pattern. The capability of the facility to operate simultaneously at two frequencies ω_1 and ω_2 also enabled investigating the cubic thermal nonlinearity, which in turn allowed generating a signal in the ionosphere with the low frequency $\Omega = 2\omega_1 - \omega_2$ without resorting to the amplitude modulation of waves directed to the ionosphere [53].

It was predicted in [54] that a natural resonance structure — an ionospheric Alfven resonator (IAR) located at altitudes of 100 – 1000 km — must exist in the ionosphere; it was experimentally discovered in [55]. At present, measurements of its parameters are widely used for diagnostics of the upper atmosphere.

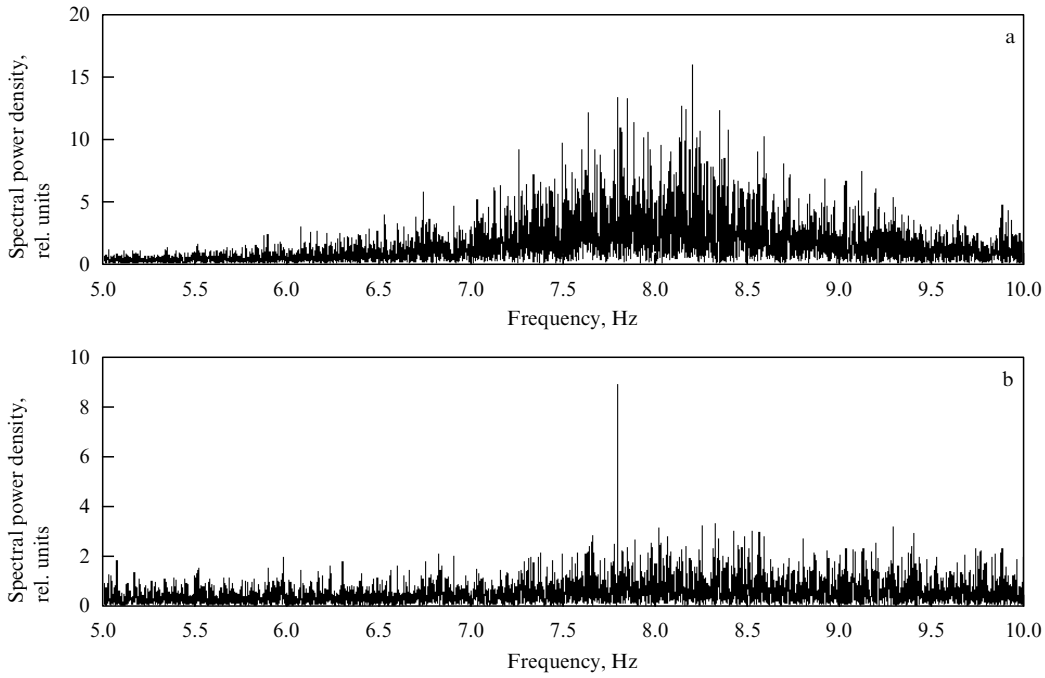

Figure 3. Spectral power densities of the signals from two detection devices (a) and spectral power density of the difference signal (b), where a 7.8 Hz signal is seen quite clearly.

The equipment and methods for measuring weak low-frequency electromagnetic radiation developed in the course of investigations are validly used for the study of the natural noise background in the $10^{-3}-10$ Hz frequency range. This range occupies a special place in geophysical research because it comprises the frequencies of the main resonances of near-earth space: the magnetohydrodynamic (MHD) resonances of the terrestrial magnetosphere, the Alfven resonances of individual geomagnetic field tubes, the Schumann resonances of the earth – ionosphere cavity, the frequencies of Alfven masers (the generators of short-pulse geomagnetic pulsations) and the ionospheric Alfven resonator frequencies. This permits investigating the dynamics of terrestrial magnetospheric processes, studying the properties of MHD waves in the IAR region at altitudes of the F ionospheric domain, studying the efficiency of IAR excitation by different sources (magnetospheric, VLF heater radiation, and energetic particle fluxes), and diagnosing the upper ionosphere at altitudes of 300 – 3000 km from the spatio-temporal behavior of the spectrum of atmospheric noise background, whose variations are related to variations in the geophysical conditions and to the large-scale structure of the electron density profile in the upper part of the F region.

The low-frequency signals generated in the ionosphere by the Sura heater in the extremely low frequency (ELF) range are used as a controllable source for the development of new methods for measuring the spatial characteristics of radio waves with frequencies below 30 kHz. In particular, a differential gradiometering method [56] was tested in 2005. The method relies on the possibility of detecting weak signals against the high-power noise background by recording the amplitude at two spatially separated points with the subsequent subtraction of the signals. For instance, because the noise from a thunderstorm is uniform on a large spatial scale, synchronous recordings made at two locations spaced several dozen or even hundreds of kilometers apart have a high degree of coherence. This enables weak emissions with small-scale coherence to be extracted and experimentally investigated (Fig. 3).

At present, research into the effect of low-frequency radio wave generation by an ionospheric source is being intensively pursued in the USA in experiments at the HAARP and HIPAS heaters. The aim of these experiments is to find possibilities for increasing the ionospheric source intensity and reliability to the level required for the solution of communication problems and for probing the earth's interior and the magnetosphere. As regards the Sura heater, the prospects of its employment rely on (i) the development of modern automated control over its parameters and operating mode; (ii) the recovery of the transmitting complex with the radiation frequency close to the electron gyrofrequency, whose operation substantially broadens the heater potentials for the CFS generation; and (iii) the development of new pulsed superpower final stages. This will furnish the possibility of continuing, at a new level, research aimed at the elaboration of practical applications of low-frequency radio wave ionospheric generation.

4. Artificial periodic irregularities

The action of high-power radio waves on ionospheric plasma is accompanied not only by the development of AIT but also by the production of ordered structures. These primarily include artificial periodic irregularities (APIs), which are produced in the field of a high-power standing radio wave resulting from the interference of an incident wave and a wave reflected from the ionosphere. In 1970, Vilenskii predicted [57] that the electron gas in the antinode of a standing wave must warm up to give rise to a periodic temperature structure with the spatial period equal to half the wavelength of the high-power radio wave. The temperature irregularities, in turn, must produce electron density irregularities.

Experiments aimed at discovering APIs were pioneered by Getmantsev early in the execution of the Zimenki heater (NIRFI) research program. These irregularities were discovered in 1975 [7]. Further investigations showed that the APIs were formed in the altitude range from 60 km to the altitude of high-power wave reflection in the ionosphere. Based on experimental and theoretical research, it was determined that the API production and relaxation mechanisms, which turned out to be substantially more complicated than predicted by Vilenskii, had a different physical nature in different ionospheric layers. In particular, the production of APIs in the altitude range D ($h \approx 50-90$ km) is due to the temperature dependence of the coefficient of electron attachment to oxygen molecules; in the E region ($h \approx 90-130$ km), the irregularities are produced due to diffusive plasma redistribution under the excess pressure of the electron component heated in the antinodes of the standing radio wave; lastly, the APIs in the F region ($h \approx 200-350$ km) are produced under the action of the ponderomotive striction force with the excitation of ion – sound oscillations [58].

Because APIs are ordered in space, the radio waves they scatter have an appreciable amplitude only if the signals arising from all irregularities in the volume under investigation are added up in phase. This imposes certain constraints on the wavelengths of a high-power transmitter and pulsed radar. The resonance scattering condition (the Bragg condition) in the case of backscattering from the APIs implies the equality $\lambda_1 = \lambda_2$, where λ_1 and λ_2 are the respective wavelengths of the high-power radiation producing the APIs in the plasma and of the radar. This circumstance gave rise to the other frequently used name of this method: resonance radio wave scattering. The condition $\lambda_1 = \lambda_2$ can be satisfied in two cases, which in fact define two possible ways of observing and recording the APIs. The first, which has been used in the majority of experiments, involves the API production and radar by waves with the same frequency and polarization. In this case, the API recording condition is the equality $f_1 = f_2$ and the scattered signal is observed from all altitudes at which the APIs are sufficiently high in amplitude. The second way requires using radio waves with different frequencies and polarizations for the production of the APIs and their radar. Then, the condition for recording the scattering from the APIs is the relation $f_1 n_1^{\mathrm{o,x}} = f_2 n_2^{\mathrm{x,o}}$, where n_1 and n_2 are the refractive indices for the ordinary (the superscript '0') and extraordinary (the superscript 'x') waves at the corresponding frequencies. For given frequencies f_1 and f_2, this condition virtually uniquely determines the electron density, which underlies the method of determining the altitude dependence of the electron density $N(h)$.

Obtaining the altitude electron density profile $N_{\mathrm{e}}(h)$ requires varying the ~ 1 MHz radar frequency about the heater transmitter frequency and recording the altitudes of the signals scattered from the APIs. An important feature of the method is the possibility of measuring the profile $N_{\mathrm{e}}(h)$ in the valley (the interlayer trough) between the regions E and F. The upper measurement limit (in altitude) is due to the altitude of high-power wave reflection and the lower limit is due to the spectral width Δf_2 of the probing pulse. For $f_1 - f_2 < \Delta f_2$, the spatial matching between the API-producing wave and its diagnostic wave is satisfied for almost all altitudes of the D region, making it difficult to determine the altitude of signal scattering. This difficulty may be overcome by measuring the phase of the scattered signal, because the phase increment with altitude is proportional to the integral electron density. This underlies the phase technique for measuring the electron density [58].

Waves with extraordinary polarization are typically used for generating APIs because such waves do not excite ionospheric plasma instabilities and therefore experience lower losses in the reflection from the F ionospheric region, with the reflected wave having more regular characteristics. As a rule, the high-power wave is radiated at frequencies $\sim 4-6$ MHz. Measurements using the resonance scattering technique are performed as follows. The action on the ionosphere is effected with the period of several dozen seconds. In each measurement cycle, to produce the APIs, the high-power transmitter operates in the cw mode for several seconds to emit waves with extraordinary polarization vertically upwards. Subsequently, the transmitter is converted to the pulsed mode to emit short (20 – 30 μs long) pulses with the same frequency and polarization. The radio pulse repetition rate is several dozen Hertz. The signals scattered from each of the probing pulses are received by an auxiliary antenna array. The requisite circularly polarized wave is extracted from the signals received and is amplified by the receiver. The amplitude of this wave is recorded in the digital form with the aid of an analog-to-digital converter in the form of sine and cosine components in the 50 – 400 km altitude range. The experiment is schematized in Fig. 4, and Fig. 5 exemplifies the recording of the signals.

The primary data processing involves calculating the signal phase and amplitude at each altitude for each heating cycle and approximating their time dependences by linear functions of the form $\ln A(t) = \ln A_0 - t/\tau$, where τ characterizes the API lifetime after switching off the heating transmitter. The understanding of the mechanisms of API formation at different altitudes has enabled developing new methods of determining the main parameters of the atmosphere and ionospheric plasma. All these methods rely on the production of APIs, their radar by probing radio ways, the reception of signals scattered by the irregularities, and the determination of altitude – temporal characteristics of the scattered signals.

The theory of API formation and the main results of the experimental ionosphere research by this technique are detailed in monograph Ref. [58]. By using APIs, it is possible to determine

- the electron density distribution with altitude, including the interlayer E-F valley (altitudes 60 – 250 km);
- the temperature and density of the atmosphere at E-region altitudes (100 – 130 km);
- the velocity of vertical motion in the D and E regions (60 – 130 km);
- the characteristic turbulent velocity at turbopause altitudes and the height of the turbopause (90 – 100 km);
- the relative density of negative oxygen ions, the density of atomic oxygen and excited molecular oxygen in the $^1\Delta_{\mathrm{g}}$ state in the D region (60 – 90 km);
- the ionic composition of the sporadic E layer (85 – 130 km);
- the electron and ion temperatures in the F region (200 – 300 km).

Apart from the characteristics listed above, the method of resonance signal scattering from the APIs also permits determining the parameters of internal gravity waves and their spectral characteristics; investigating the nonuniform structure of the lower ionosphere, including the stratification of the regular E layer; discovering weak sporadic ionization

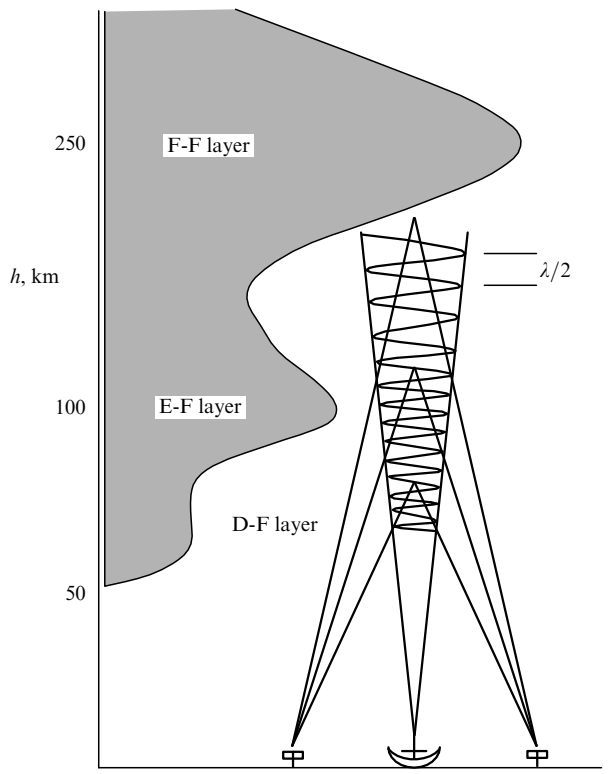

Figure 4. Scheme for the production of artificial periodic irregularities of ionospheric plasma and their radar by pulsed signals.

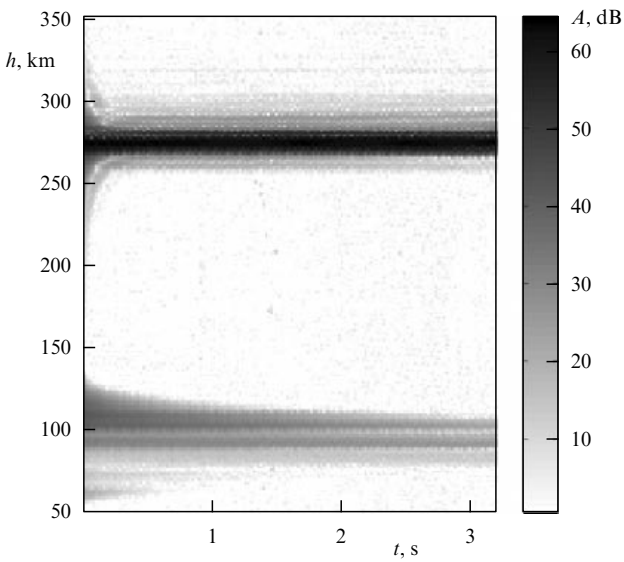

Figure 5. Example of the recording of a signal scattered from APIs. The maximum signal arises from the E region at the altitudes 100 – 130 km and the weak signal from the D region (60 – 80 km). At the altitude 270 km is the specularly reflected signal from the F layer and below a rapidly decaying ion sound.

layers, which escape detection by ordinary ionosondes, and additional layers in electron density profiles, beginning with the lower part of the D region and up to the altitude of the F-layer maximum; and investigating the features of sunrise and sunset phenomena in the D region.

The ionosphere investigation method with the help of APIs continues to develop. Proposed recently was a new way of determining the electron density from API relaxation time measurements at two sufficiently spaced frequencies [59]. This opens the way to a more precise measurement of the altitude profile of the electron density in the E region, as well as the temperature and density of the neutral atmosphere at the altitudes 90 – 115 km. This also opens up the possibility of determining the ambipolar diffusion coefficient and the turbulent motion velocity independently of one another.

By comparing the API method with other methods of remote ionospheric probing, it may be concluded that this method is vastly superior to them in information value. The API-based methods of plasma parameter determination afford high temporal resolution, which favorably distinguishes them, e.g., from the method of incoherent scattering, and may rival rocket research, substantially exceeding it in economy. The method is environmentally clean, because it does not introduce additional impurities into the atmosphere. In the measurements, the heating of the electron plasma component is insignificant and does not disturb the thermal balance of the neutral atmosphere. It is significant that all API-based methods of plasma diagnostics are easily combined into a common complex technique, making it possible to pursue research and monitor the ionosphere in a wide altitude range, from the D region to the F region [58].

5. Conclusion

Our report outlines the main findings of research involving the modification of the ionosphere by high-power HF radio waves, which was carried out from 1973 to 2006, first using the Zimenki heater and then, since 1981, the Sura heater. The new effects discovered in these experiments have far exceeded the expected phenomena due to ohmic plasma heating by high-power radio waves. The experiments conducted have enabled investigating the properties of different instabilities responsible for the generation of artificial ionospheric turbulence; studying the generation mechanisms of combination frequency signals and pointing out the areas of their practical use; and developing new radiophysical methods for the measurement of ionosphere parameters and plasma turbulence with the help of artificial periodic irregularities, stimulated electromagnetic emission, and aspect scattering of HF and VHF radio waves. This has opened up new vistas for research in which the ionosphere will be harnessed as a natural plasma laboratory that allows the pursuance of experiments to study a wide range of problems in plasma physics, geophysics, and space physics.

This work was supported by the Russian Foundation for Basic Research (grant Nos. 04-02-17333, 04-02-16612, 05-02-16493, 04-05-64140, 05-05-64111, 05-05-64304, and 06-05-64995) and INTAS (grant No. 03-51-5583).

References

1. Genkin L G , Erukhimov L M *Phys. Rep.* **186** 97 (1990)
2. Bailey V A *Philos. Mag.* **23** 929 (1937)
3. Ginzburg V L, Gurevich A V *Usp. Fiz. Nauk* **70** 201, 393 (1960) [*Sov. Phys. Usp.* **3** 115, 175 (1960)]
4. *Radio Sci.* **9** (11) (1974)
5. Getmantsev G G et al. *Pis'ma Zh. Eksp. Teor. Fiz.* **18** 621 (1973) [*JETP Lett.* **18** 364 (1973)]
6. Getmantsev G G et al. *Pis'ma Zh. Eksp. Teor. Fiz.* **20** 229 (1974) [*JETP Lett.* **20** 101 (1974)]
7. Belikovich V V et al. *Pis'ma Zh. Eksp. Teor. Fiz.* **22** 497 (1975) [*JETP Lett.* **22** 243 (1975)]
8. *J. Atm. Terr. Phys.* **44** (12) (1982)

9. *J. Atm. Terr. Phys.* **47** (12) (1985)
10. *J. Atm. Solar-Terr. Phys.* **59** (18) (1997)
11. *Izv. Vyssh. Uchebn. Zaved., Radiofiz.* **37** (5) (1994)
12. *Izv. Vyssh. Uchebn. Zaved., Radiofiz.* **42** (7, 8) (1999)
13. *Izv. Vyssh. Uchebn. Zaved., Radiofiz.* **48** (9) (2005)
14. Frolov V L et al. *J. Atm. Solar-Terr. Phys.* **59** 2317 (1997)
15. Vas'kov V V, Gurevich A V *Izv. Vyssh. Uchebn. Zaved., Radiofiz.* **16** 188 (1973)
16. Grach S M et al. "Teplovaya parametricheskaya neustoichivost' v ionosfernoi plazme" ("Thermal parametric instability in ionospheric plasma"), in *Teplovye Nelineinye Yavleniya v Plazme* (Thermal Nonlinear Phenomena in Plasma) (Executive Ed. V Yu Trakhtengerts) (Gorky: IPF AN SSSR, 1979) p. 46
17. Vas'kov V V et al. "Samofokusirovochnaya i rezonansnaya neustoichivosti v ionosfere" ("Self-focusing and resonance ionospheric instabilities"), in *Teplovye Nelineinye Yavleniya v Plazme* (Thermal Nonlinear Phenomena in Plasma) (Executive Ed. V Yu Trakhtengerts) (Gorky: IPF AN SSSR, 1979) p. 81
18. Litvak A G *Izv. Vyssh. Uchebn. Zaved., Radiofiz.* **11** 1433 (1968)
19. Gurevich A V, Zybin K P, Carlson C S *Izv. Vyssh. Uchebn. Zaved., Radiofiz.* **48** 772 (2005) [*Radiophys. Quantum Electron.* **48** 686 (2005)]
20. Erukhimov L M et al. *Izv. Vyssh. Uchebn. Zaved., Radiofiz.* **30** 208 (1987) [*Radiophys. Quantum Electron* **30** 156 (1987)]
21. Nasyrov A M *Rasseyanie Radiovoln Anizotropnymi Ionosfernymi Neodnorodnostyami* (Kazan: Izd. Kazan. Univ., 1991)
22. Frolov V L *Int. J. Geomagn. Aeronom.* **4** (2) 159 (2003)
23. Yampolski Y M et al. *J. Geophys. Res.* **102** (A4) 7461 (1997)
24. Blagoveshchenskaya N F et al. *Ann. Geophys.* **24** 2333 (2006)
25. Koloskov A V et al. *J. Geophys. Res.* **107** (A7) SIA1 (2002)
26. Uryadov V P et al. *Izv. Vyssh. Uchebn. Zaved., Radiofiz.* **47** 722 (2004) [*Radiophys. Quantum Electron* **47** 646 (2004)]
27. Ponomarenko P V, Leyser T B, Thidé B *J. Geophys. Res.* **104** (A5) 10081 (1999)
28. Kagan L M et al. *Radio Phys. Radio Astron.* **11** 221 (2006)
29. Belikovich V V et al., in *XIII Vsesoyuz. Konf. po Rasprostraneniyu Radiovoln, Gor'kii, Iyun' 1981: Tezisy Dokladov* (XIIIth All-Union Conference on Radio Wave Propagation, Gorky, June 1981: Abstracts) Pt. 1 (Moscow: Nauka, 1981) p. 107
30. Thidé B, Kopka H, Stubbe P *Phys. Rev. Lett.* **49** 1561 (1982)
31. Leyser T B *Space Sci. Rev.* **98** 223 (2001)
32. Frolov V L et al. *Geophys. Res. Lett.* **28** 3103 (2001)
33. Sergeev E N et al. *Izv. Vyssh. Uchebn. Zaved., Radiofiz.* **41** 313 (1998)
34. Sergeev E N et al. *Izv. Vyssh. Uchebn. Zaved., Radiofiz.* **42** 619 (1999)
35. Frolov V L et al. *Izv. Vyssh. Uchebn. Zaved., Radiofiz.* **48** 110 (2005)
36. Frolov V L, Sergeev E N, Stubbe P *Izv. Vyssh. Uchebn. Zaved., Radiofiz.* **45** 121 (2002)
37. Frolov V L et al. *Izv. Vyssh. Uchebn. Zaved., Radiofiz.* **49** 643 (2006) [*Radiophys. Quantum Electron* **49** 579 (2006)]
38. Bakhmet'eva N V et al. *Geomagnetizm Aeronomiya* **32** (3) 180 (1992)
39. Grach S M et al. *Ann. Geophys.* **20** 1687 (2002)
40. Tereshchenko E D et al. *Phys. Lett. A* **325** 381 (2004)
41. Nygrén T et al. *Radio Sci.* **32** 2359 (1997)
42. Frolov V L et al. *Ann. Geophys.* (2006) (submitted for publ.)
43. Uryadov V P et al. *J. Atm. Terr. Phys.* **57** 1263 (1995)
44. Frolov V L et al. "Artificial ionospheric turbulence and radio wave propagation", in *RF Ionospheric Interactions Workshop. 25 – 28 April 2006, Santa Fe, New Mexico, USA* Summary of presentations on CD No. 7
45. Belikovich V V et al. *Usp. Fiz. Nauk* **113** 732 (1974) [*Sov. Phys. Usp.* **17** 615 (1975)]
46. Kotik D S, Trakhtengerts V Yu *Pis'ma Zh. Eksp. Teor. Fiz.* **21** 114 (1975) [*JETP Lett.* **21** 51 (1975)]
47. Kapustin I N et al. *Pis'ma Zh. Eksp. Teor. Fiz.* **25** 248 (1977) [*JETP Lett.* **25** 228 (1977)]
48. Getmantsev G G et al. "Yavlenie generatsii elektromagnitnykh voln ionosfernymi tokami pod vozdeistviem na ionosferu modulirovannogo korotkovolnovogo radioizlucheniya" ("Effect of electromagnetic wave generation by ionospheric currents under exposure of the ionosphere to modulated short-wave radio-frequency radiation") *Bull. Izobret.* (8) 3 (1981)
49. Bellyustin N S et al. *Izv. Vyssh. Uchebn. Zaved., Radiofiz.* **18** 1323 (1975)
50. Kotik D S et al. "K teorii signalov kombinatsionnykh chastot" ("On the theory of combination frequency signals"), in *Nelineinye Yavleniya v Ionosfere* (Nonlinear Phenomena in the Ionosphere) (Murmansk: Izd. PGI KF AN SSSR, 1979) p. 114
51. Belyaev P P et al. *Izv. Vyssh. Uchebn. Zaved., Radiofiz.* **30** 248 (1987)
52. Kotik D S et al. *Izv. Vyssh. Uchebn. Zaved., Radiofiz.* **37** 783 (1994)
53. Kotik D S, Ermakova E N *J. Atm. Solar-Terr. Phys.* **60** 1257 (1998)
54. Polyakov S V, Rappoport V O *Geomagnetizm Aeronomiya* **21** 816 (1981)
55. Belyaev P P et al. *J. Atm. Terr. Phys.* **52** 781 (1990)
56. Polyakov S V et al. *Izv. Vyssh. Uchebn. Zaved., Radiofiz.* (2006) (in press)
57. Vilenskii I M *Dokl. Akad. Nauk SSSR* **191** 1041 (1970)
58. Belikovich V V et al. *Issledovanie Ionosfery s Pomoshch'yu Iskusstvennykh Periodicheskikh Neodnorodnostei* (Investigation of the Ionosphere by Artificial Periodic Irregularities) (Nizhny Novgorod: IPF RAN, 1999) p. 155
59. Belikovich V V et al. *Izv. Vyssh. Uchebn. Zaved., Radiofiz.* **49** 744 (2006)